Electronic Supplementary Information

Surface Coating Induced Room-temperature Phosphorescence in Flexible Organic Single Crystals

Prodipta Samadder,[a] Khalid Naim,[a] Subash Chandra Sahoo,[b] Prakash P. Neelakandan[a*]

[a] Institute of Nano Science and Technology, Knowledge City, Sector 81, Mohali 140306.
Email: ppn@inst.ac.in
[b] Department of Chemistry, Panjab University, Sector 14, Chandigarh 160014.

EXPERIMENTAL DETAILS

S1. General Techniques

All the experiments were carried out at room temperature (25 ± 1 ^{o}C) unless otherwise mentioned. Melting points (m.p.) were measured in open capillaries with a Stuart (automatic melting point SMP50) apparatus and were uncorrected. NMR spectra were measured on a 400 MHz Bruker Avance II Neo spectrometer. NMR spectra were internally referenced to the residual solvent signal at δ 7.26 ppm for $CDCl_3$. Hexafluorobenzene was used as the internal standard for ^{19}F NMR spectra in $CDCl_3$, and the reference peak position for ^{19}F was taken as δ –164.9 ppm.[1] Absorption spectra were recorded on a Shimadzu UV-2600 UV-Vis spectrophotometer in 3 mL quartz cuvettes having a path length of 1 cm. For solid samples, reflectance spectra were collected and transformed into absorbance through Kubelka-Munk transformation. Fluorescence spectra were recorded on a Fluorolog 3-221 fluorimeter equipped with a 450 W Xenon lamp. Fluorescence lifetimes were measured using Fluorolog TCSPC Horiba FL-1057, and phosphorescence lifetime and gated emission were measured by FL-1040A phosphorimeter used with the Fluorolog-3 and Nanolog spectrofluorometers. High-resolution mass spectra (HRMS) were measured by using Waters Corporation MALDI-TOF Synapt XS HD Mass Spectrometer. Field emission scanning electron microscope (FESEM) images were captured using Jeol JSM-7610FPlus FESEM, and EDX analysis was performed with Z2-i7 analyser. Crystals were observed with an optical microscope (Olympus BX53F).

S2. Materials.

4,4’-Dimethoxy benzophenone (**1**), 1-hydroxy-2-naphthaldehyde (**A**) and *o*-toluidine (**B**) were purchased from TCI Chemicals. Boron trifluoride diethyletherate was purchased from Sigma-Aldrich. Silica gel (60-120 mesh), methanol, dichloromethane (DCM), hexane, and trimethylamine were purchased locally. Solvents were distilled and dried before use.

S3. Synthesis of 5.

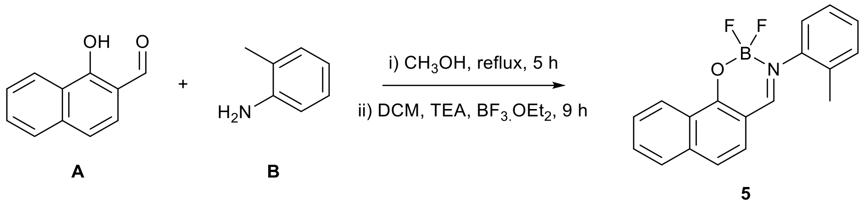

Scheme S1. Synthesis of compound **5**.

1-Hydroxy-2-naphthaldehyde (**A**, 250 mg, 1.45 mmol) was dissolved and stirred in methanol (4 mL). Then *o*-toluidine (**B**, 160 µL, 1.50 mmol) was added slowly, and the mixture was refluxed for 5 hours at 60 °C. The solvent was evaporated off in a rotary evaporator to obtain an orange-yellow residue. The orange-yellow powder washed with hexane and dried. After that it dissolved in anhydrous DCM (50 mL). Then the solution was cooled to 0 °C in an ice bath and triethylamine (0.213 mL) was added with continuous stirring. The reaction mixture was then stirred for 30 minutes, followed by the addition of $BF_3·OEt_2$ (0.472 mL). After stirring the reaction mixture for 9 hours at 25 ^{o}C, the solvents were evaporated off in a rotary evaporator and the crude product was purified by column chromatography on silica gel by using a mixture of DCM and hexane (40:60) as the eluent to yield **5** in 95 % yield as a bright greenish-yellow powder. M.p.: 206-207 °C; ^{1}H NMR (400 MHz, 298 K,$CDCl_3$) δ (ppm) 8.66-8.64 (d, 1H, J = 8 Hz), 8.27-8.26 (m, 1H), 7.82-7.80 (m, 1H), 7.74-7.70 (m, 1H), 7.63-7.59 (m, 1H), 7.42-7.39 (m, 2H), 7.37-7.29 (m, 4H), 2.34(3H, s); ^{13}C NMR (100 MHz, 298 K, $CDCl_3$) δ (ppm) 165.50, 161.06, 141.62, 138.96, 132.88, 131.71, 131.59, 129.08, 127.87, 126.93, 126.87, 126.13, 125.66, 125.60, 125.13, 120.55, 17.88; ^{19}F NMR (376 MHz, $CDCl_3$): δ (ppm) -136.35 (m, 2F); HRMS (ESI-MS) m/z calculated for $C_{18}H_{14}BF_2NO$ [M+Na]$^+$: 332.1100; found: 332.1066.

S4. Growing single crystals of 1

Single crystals of **1** were grown by the slow diffusion of hexane into dichloromethane (DCM) solutions of **1**. 25 mg of **1** was dissolved in 3 mL of DCM in a 15 mL glass vial. To this vial 10 mL hexane was added slowly, and the cap of the glass vial was closed tightly. Transparent and long tape-like crystals of **1** were obtained after 4-5 days.

S5. Coating of crystals of 1 with molecules 2-5.

Crystal of **1** was held with a tweezer, and a solution of **2**-**5** in DCM was drop-cast on the crystal with a syringe. The crystals were then allowed to dry for a few seconds and used for further studies.

S6. Single-Crystal X-ray Analysis

A suitable single crystal of **1** was selected and mounted on Hampton cryoloops. All geometric and intensity data for the crystals were collected using a Super-Nova (Mo) X-ray diffractometer equipped with a micro-focus sealed X-ray tube Mo-Kα (λ = 0.71073 Å) X-ray source and a HyPix3000 detector with increasing ω (width of 0.3 per frame) at a scan speed of either 5 or 10 s/frame. The CrysAlisPro software was used for data acquisition and data extraction. Using Olex2, the structure was solved with the SIR2004 structure solution program using direct methods and refined with the ShelXL refinement package using least squares minimisation.[2,3] All non-hydrogen atoms were refined with anisotropic thermal parameters. Detailed crystallographic data and structural refinement parameters are summarised in Table S1. Bond lengths and bond angles are listed in Tables S4 and S5. CCDC2299361 contains the supplementary crystallographic data. These data can be obtained free of charge from the Cambridge Crystallographic Data Centre.

S7. Hirshfeld Analysis

Important intermolecular interactions within the crystal structure of **1** were identified through Hirshfeld surface analysis using Crystal Explorer 17.5. The Hirshfeld surface is defined as a set of points in the 3D space where the ratio of promolecule and procrystal electron densities is equal to 0.5.[4] The exploration of intermolecular contacts is provided by mapping normalised contact distances (d_{norm}), which is a function of the closest distance from the point to the nuclei interior (d_i) and exterior (d_e) to the surface as well as on the van der Waals radii (r^{vdw}). Hirshfeld surface d_{norm} displays various intermolecular interactions in terms of red, blue, and white schemes, in which red denotes short contacts, white highlights interactions operating within the range of van der Waals radii, and blue represents long-range contacts. 2D fingerprints were generated by deriving the Hirshfeld surface by plotting the fraction of points on the surface as the function of d_i and d_e, which provides a visual summary of intermolecular contacts within the crystal.

S8. Face Indexing.

Face indices of the crystals of **1** was identified and described based on SCXRD data and matched with predicted BFDH morphology. Prior to face indexing, the crystals were centered, and the shape was defined with respect to both *hkl* and *xyz* values. The final faces were indexed appropriately using both the drag and point methods of the CrysAlisPro software.

S9. Calculation of Crystal Bending strain

Vacuum grease was used to hold a crystal from one side while a force was applied on the crystal using a soft paintbrush from the opposite side. All bending experiments were carried out using a graduated (0.5 cm scale) glass slide for measurements and recorded using a digital camera. The thickness (t) of the crystal was measured prior to bending, while the length (L) and maximal displacement (h_{max}) were measured at the point of maximal curvature. The radius of the curvature (R) was calculated from the geometric construction given as follows:

$$R \ = \ (R - h_{\mathrm{max}})^2 + \left(\frac{L}{2}\right)^2$$

$$R = \frac{h_{max}^2 + L^2/4}{2h_{max}}$$

The bending strain was calculated using Euler-Bernoulli equation[5] (bending of organic crystals could be regarded as a pure bending process without any shear components):

$$\varepsilon\ (\%) = \frac{t\ /\ 2}{R} \times 100$$

S10. Nanoindentation

Nanoindentation was carried out using Ti-950 Tribo Indenter (Hysitron Inc., Minneapolis, MN) equipped with a three-sided pyramidal Berkovich diamond indenter (tip end radius 150 nm). For quasi-static indentation characterisation of mechanical properties, namely Young's modulus and hardness, the nano-mechanical response of crystals of **1** was studied by twodimensional nanoindentation profiling across the kink. The resultant loading-indentation depth curves obtained as a response of the material to indentation were used to obtain the elastic modulus in fixed load mode (FLM). The crystals were impacted at ⊥ (100), and each indentation was performed with loading/unloading cycles until a peak load of 0.5 and 1.0 mN with a hold time of 10 s at peak load. The regions for testing were identified using an optical microscope integrated into the nanoindentation system. The indentation sequence follows the indenter pressing with pre-defined load or depth, holding in the terminal position followed by withdrawal. The resultant loading indentation depth curves obtained as a response of the material to indentation were used to obtain the elastic modulus in fixed load mode (FLM). All the experiments were repeated with multiple crystals, and the value of the elastic modulus E of the crystals was extracted from the load-displacement (*P*-*h*) curves and averaged. The *P*-*h* curves obtained were analysed using the standard Oliver- Pharr method to extract the elastic modulus and hardness of the crystal, where the hardness was calculated from the peak load divided by the contact area of the indenter.[5,6]

S11. Optical Waveguide

The light propagation through the crystals of **1** and **5@1** was studied using a supercontinuum source with a spectral filter of λ = 365 nm for straight crystal and bent crystal. The light was focused using a plano-convex lens (f = 35 mm) to a single crystal of **1** and **5@1**. The reflected signal from the sample was collected by the same lens and directed to a monochrome sCMOS camera through a focusing lens. The camera captures the image of the crystal illuminated by a flash lamp. This helps to locate the excitation beam spot on the crystal. After this, the flash lamp was switched off, and the beam propagating through the length of the crystal can be seen through the naked eye. The crystal was further bent to a "U" shape, but the light intensity remained nearly constant, demonstrating the optical waveguiding behaviour of the sample. The light emerging out from one end of the crystal was collected using a focusing lens (f = 35 mm) and directed to a CCD camera. Optical loss coefficients (OLCs) of the straight and bent crystals of **1** and **5@1** were calculated by following a reported procedure.[7] The crystal was irradiated in a direction perpendicular to its long axis at different positions with a 365 nm laser from a Ti:sapphire regenerative amplifier (Astrella, Coherent) operated at 800 nm with a repetition rate of 1 kHz and pulse duration of ∼35 fs. The light was collected at the tip of the crystal that was manually aligned with a micromanipulator to the end of an optical fibre connected to a StellerNet BLUE-Wave spectrometer.

S12. Computational Details

Ground State (S_0) of **1** and **5** were optimized using density functional theory (DFT) and electronic absorption spectra was calculated using time-dependent density functional theory (TD-DFT) as implemented in the Gaussview 06 software.[8] Ground state (S_0) optimization and frequency calculation was performed employing B3LYP exchange functional with 6-31++g(d,p) basis set. While the excited state calculations were also performed B3LYP exchange-correlation functional with the same basis sets as mentioned before. Ground state frequency calculation was performed to confirm the absence of any unstable normal mode. The first singlet excited state (S_1) was optimized at the TD-DFT level of theory. While the first triplet excited states (T_1) were also optimized at the TD-DFT level of theory within the Tamm-Dancoff approximation (TDA) to overcome the triplet instability issue. On the basis of the Frank-Condon principle, the absorption properties were evaluated using the optimized S_0 state structure. The Gaussview 06 software was used in all the DFT and TDDFT calculations.

The interaction between **1** and **5** was calculated using DFT as implemented in the Gaussview 06 software. Geometry optimization was performed employing B3LYP exchange functional with 6-31++g(d,p) basis set.

References

1 I. E. Kareev, I. V. Kuvychko, S. F. Lebedkin, S. M. Miller, O. P. Anderson, K. Seppelt, S. H. Strauss and O. V. Boltalina, *J. Am. Chem. Soc.*, 2005, **127**, 8362–8375.

2 O. V. Dolomanov, L. J. Bourhis, R. J. Gildea, J. a. K. Howard and H. Puschmann, *J. Appl. Cryst.*, 2009, **42**, 339–341.

3 G. M. Sheldrick, *Acta Crystallogr. A Found. Adv.*, 2015, **71**, 3–8.

4 J.-R. Wang, M. Li, Q. Yu, Z. Zhang, B. Zhu, W. Qin and X. Mei, *Chem. Commun.*, 2019, **55**, 8532–8535.

5 W. C. Oliver and G. M. Pharr, *J. Mater. Res.*, 2004, **19**, 3–20.

6 W. C. Oliver and G. M. Pharr, *J. Mater. Res.*, 1992, **7**, 1564–1583.

7 L. Catalano, D. P. Karothu, S. Schramm, E. Ahmed, R. Rezgui, T. J. Barber, A. Famulari and P. Naumov, *Angew. Chem., Int. Ed.*, 2018, **57**, 17254–17258.

8 GaussView, Version 6, Dennington, Roy; Keith, Todd A.; Millam, John M. Semichem Inc., Shawnee Mission, KS, 2016.

Table S1. Crystal data and structure refinement parameters for the compound **1**.

CCDC no	2299361
Empirical formula	$C_{30}H_{28}O_6$
Formula weight	484.52
Temperature/K	293(2)
Crystal system	triclinic
Space group	$P\bar{1}$
a/Å	9.5504(4)
b/Å	9.6216(4)
c/Å	14.9202(5)
α/°	76.429(3)
β/°	78.195(3)
γ/°	70.242(4)
Volume/Å^3	1242.47(9)
Z	2
ρcalcg/cm3	1.295
μ/mm-1	0.090
F(000)	512.0
Crystal size/mm3	0.021 × 0.018 × 0.015
Radiation	MoKα (λ = 0.71073)
2Θ range for data collection/°	6.616 to 52.744
Index ranges	$-11 \le h \le 11$, $-12 \le k \le 11$, $-18 \le l \le 18$
Reflections collected	14173
Independent reflections	5034 [R_{int} = 0.0347, R_{sigma} = 0.0409]

Data/restraints/parameters	5034/0/329
Goodness-of-fit on F2	1.037
Final R indexes [I>=2σ (I)]	R_1 = 0.0487, wR_2 = 0.1127
Final R indexes [all data]	R_1 = 0.0785, wR_2 = 0.1303
Largest diff. peak/hole / e Å^{-3}	0.15/-0.25

Table S2. Percentage of intermolecular interactions present in the crystals of **1** derived from Hirshfeld surface analysis.

Interaction	**1**
% C···H	29.4
% C···C	0
% H···H	42.5
% O···H	27.9
% C···O	0.2
ρ = [(%C···H)/(%C···C)]	Infinite

Table S3. Fractional Atomic Coordinates (×10^4) and Equivalent Isotropic Displacement Parameters (Å^2×10^3) for compound **1**. U_{eq} is defined as 1/3 of the trace of the orthogonalized U_{IJ} tensor.

Atom	x	y	z	U(eq)
O1	2123.4(11)	1470.2(12)	6532.3(7)	58.3(3)
O6	1607.9(12)	3648.9(12)	9699.6(7)	61.8(3)
O4	7844.2(13)	3530.8(12)	3520.7(7)	63.6(3)
O3	8176.1(13)	1250.2(12)	335.7(7)	67.5(3)
O5	7790.8(13)	38.8(12)	7663.7(7)	72.3(4)
O2	2148.0(14)	5047.7(13)	2398.0(7)	80.9(4)
C24	5470.1(17)	1876.4(16)	7953.7(10)	44.8(4)
C14	5106.0(17)	1653.6(16)	2203.7(9)	48.1(4)
C5	2817.0(17)	3216.9(16)	3719.5(10)	45.4(4)
C2	2268.7(17)	2093.3(16)	5614.2(10)	44.8(4)

C20	7059.7(16)	1797.4(16)	6333.4(10)	44.3(4)
C6	4003.0(16)	2376.9(16)	4229.2(10)	47.4(4)
C21	6642.8(16)	3341.0(16)	5981.9(10)	47.4(4)
C27	2903.1(17)	3008.8(16)	9169(1)	46.0(4)
C29	4129.8(17)	2773.3(16)	7620.5(10)	47.6(4)
C19	7782.4(16)	834.2(16)	5708.6(10)	49.6(4)
C7	3728.7(16)	1833.0(16)	5163.1(10)	47.7(4)
C22	6939.3(16)	3874.7(16)	5049.8(10)	49.6(4)
C9	4460.2(17)	3207.1(16)	2120.1(9)	47.0(4)
C17	7635.9(16)	2885.5(17)	4432.4(10)	46.0(4)
C25	5475.8(17)	1550.1(16)	8912.5(10)	50.4(4)
C3	1075.1(17)	2926.6(15)	5124.6(10)	50.2(4)
C23	6837.8(17)	1170.0(16)	7344.3(10)	49.5(4)
C4	1369.1(17)	3482.6(16)	4187(1)	50.5(4)
C12	6961.1(17)	1970.2(17)	893.7(10)	48.8(4)
C28	2867.1(17)	3321.2(16)	8219.4(10)	49.4(4)
C13	6318.4(17)	1048.0(16)	1592.3(9)	49.4(4)
C18	8054.0(16)	1356.4(16)	4768.1(10)	50.6(4)
C26	4218.1(18)	2107.9(16)	9519.3(10)	50.6(4)
C8	3075.5(18)	3900.0(17)	2723.3(10)	52.9(4)
C10	5100.9(19)	4109.9(17)	1407.4(10)	55.1(4)
C11	6344.5(19)	3513.5(18)	802(1)	56.6(4)
C1	653.7(19)	1744(2)	7046.3(11)	74.1(5)
C16	8528(2)	2564(2)	2855.6(10)	76.7(6)
C30	1551(2)	3308(2)	10687.8(10)	82.5(6)
C15	8869(2)	2130(2)	-414.0(12)	90.8(7)

Table S4. Anisotropic Displacement Parameters ($Å^2×10^3$) for compound **1**. The anisotropic displacement factor exponent takes the form: $-2\pi^2[h^2a^{*2}U_{11}+2hka^*b^*U_{12}+…]$.

Atom	**U_{11}**	**U_{22}**	**U_{33}**	**U_{23}**	**U_{13}**	**U_{12}**
O1	47.7(7)	70.8(8)	49.7(6)	-9.5(5)	-3.4(5)	-12.1(6)
O6	57.0(7)	69.0(8)	49.4(6)	-8.2(6)	-3.0(5)	-10.3(6)
O4	73.0(8)	59.4(7)	49.6(7)	-8.6(6)	-6.5(6)	-11.0(6)
O3	59.9(8)	70.0(8)	59.7(7)	-6.8(6)	3.9(6)	-13.5(6)
O5	60.6(8)	62.8(8)	70.8(8)	5.0(6)	-10.8(6)	-0.2(7)
O2	83.4(9)	61.6(8)	68.4(8)	-1.5(6)	-13.7(7)	10.6(7)
C24	46.9(9)	39.9(8)	48.5(9)	-4.2(7)	-9.9(7)	-15.0(7)
C14	55.7(10)	41.1(9)	48.1(9)	-3.8(7)	-7.1(8)	-18.2(8)
C5	46.3(9)	38.9(8)	51.9(9)	-12.5(7)	-7.9(7)	-10.4(7)
C2	44.9(9)	43.5(9)	47.6(9)	-12.5(7)	-6.9(7)	-12.1(7)
C20	40.0(9)	41.9(9)	52.4(9)	-8.5(7)	-8.2(7)	-13.2(7)
C6	40.1(9)	49.1(9)	53.3(10)	-14.8(7)	-4.7(7)	-11.2(7)
C21	49.7(9)	40.4(9)	53.8(9)	-14.1(7)	-5.0(7)	-13.1(7)
C27	48.6(10)	41.8(9)	47.5(9)	-5.1(7)	-6.8(8)	-15.6(8)
C29	51.7(10)	45.8(9)	45.6(9)	-3.7(7)	-12.4(8)	-14.8(8)
C19	44.8(9)	37.5(8)	65.2(10)	-8.4(8)	-10.9(8)	-9.4(7)
C7	38.9(9)	50.3(9)	53.6(10)	-13.8(7)	-11.4(7)	-7.3(7)
C22	50.7(10)	36.1(8)	60.3(10)	-7.2(7)	-9.5(8)	-10.9(7)
C9	54.2(10)	42.9(9)	45.6(9)	-6.2(7)	-11.2(7)	-15.6(8)
C17	40.9(9)	47.3(9)	50.0(9)	-7.5(8)	-9.4(7)	-12.6(7)
C25	50.9(10)	46.5(9)	55(1)	-1.2(7)	-17.6(8)	-15.4(8)
C3	37.6(9)	49.1(9)	62.2(10)	-16.3(8)	-5.8(7)	-7.4(7)
C23	46.4(10)	41.5(9)	60.6(10)	-3.9(8)	-12.9(8)	-13.8(8)
C4	45.1(9)	43.3(9)	60.7(10)	-10.9(7)	-16.9(8)	-3.8(7)
C12	48.7(10)	53.2(10)	43.8(9)	-6.0(8)	-9.8(8)	-14.4(8)
C28	47.9(10)	46.6(9)	51.0(9)	-3.0(7)	-14.3(8)	-10.6(8)

C13	58(1)	39.4(8)	49.2(9)	-5.6(7)	-9.9(8)	-12.9(8)
C18	47.2(10)	46.8(10)	57.9(10)	-17.6(8)	-5.8(8)	-9.7(8)
C26	57.9(11)	51.2(10)	43.4(9)	-1.1(7)	-13.5(8)	-18.3(8)
C8	60.3(11)	39.8(9)	57.4(10)	-8.3(8)	-16.1(9)	-9.3(8)
C10	67.3(11)	39.5(9)	57.2(10)	-2.9(8)	-14.5(9)	-14.9(8)
C11	66.7(11)	51.9(10)	52.5(10)	1.0(8)	-7.6(9)	-27.2(9)
C1	56.2(12)	95.8(14)	59.2(11)	-15.7(10)	5.1(9)	-15.3(10)
C16	87.4(14)	81.2(13)	52.9(10)	-19.9(9)	-1.2(9)	-14.5(11)
C30	79.3(14)	96.7(15)	50.3(11)	-9.3(10)	-0.2(9)	-7.4(11)
C15	79.2(14)	98.2(16)	77.8(13)	-2.4(11)	17.8(11)	-30.6(12)

Table S5. Bond lengths for compound **1**.

Atom	Atom	Length/Å	Atom	Atom	Length/Å
O1	C2	1.3594(16)	C2	C3	1.3870(19)
O1	C1	1.4255(17)	C20	C21	1.3997(19)
O6	C27	1.3599(17)	C20	C19	1.3835(19)
O6	C30	1.4272(16)	C20	C23	1.4875(19)
O4	C17	1.3608(16)	C6	C7	1.3731(18)
O4	C16	1.4265(18)	C21	C22	1.3712(17)
O3	C12	1.3606(17)	C27	C28	1.3827(17)
O3	C15	1.4273(18)	C27	C26	1.386(2)
O5	C23	1.2266(16)	C29	C28	1.3715(19)
O2	C8	1.2258(16)	C19	C18	1.3774(18)
C24	C29	1.3938(19)	C22	C17	1.3892(19)
C24	C25	1.3915(18)	C9	C8	1.484(2)
C24	C23	1.483(2)	C9	C10	1.3854(19)
C14	C9	1.3968(19)	C17	C18	1.3833(19)
C14	C13	1.3688(18)	C25	C26	1.378(2)
C5	C6	1.3998(19)	C3	C4	1.3826(18)

C5	C4	1.3835(19)	C12	C13	1.3867(18)
C5	C8	1.4843(19)	C12	C11	1.385(2)
C2	C7	1.3853(19)	C10	C11	1.378(2)

Table S6. Bond angles for compound **1**.

Atom	Atom	Atom	Angle/˚	Atom	Atom	Atom	Angle/˚
C2	O1	C1	118.38(11)	C21	C22	C17	120.34(13)
C27	O6	C30	118.58(12)	C14	C9	C8	122.35(13)
C17	O4	C16	117.85(12)	C10	C9	C14	117.78(14)
C12	O3	C15	118.56(13)	C10	C9	C8	119.75(14)
C29	C24	C23	123.18(13)	O4	C17	C22	115.60(13)
C25	C24	C29	117.67(14)	O4	C17	C18	124.96(14)
C25	C24	C23	118.99(13)	C18	C17	C22	119.43(13)
C13	C14	C9	120.91(14)	C26	C25	C24	121.85(14)
C6	C5	C8	122.11(14)	C4	C3	C2	119.02(14)
C4	C5	C6	117.93(13)	O5	C23	C24	120.38(14)
C4	C5	C8	119.84(13)	O5	C23	C20	118.93(14)
O1	C2	C7	115.55(13)	C24	C23	C20	120.67(13)
O1	C2	C3	124.50(13)	C3	C4	C5	122.00(14)
C7	C2	C3	119.95(13)	O3	C12	C13	115.55(13)
C21	C20	C23	122.82(13)	O3	C12	C11	124.90(14)
C19	C20	C21	117.70(13)	C11	C12	C13	119.55(14)
C19	C20	C23	119.39(13)	C29	C28	C27	120.54(14)
C7	C6	C5	120.71(14)	C14	C13	C12	120.46(14)
C22	C21	C20	120.96(13)	C19	C18	C17	119.71(14)
O6	C27	C28	115.95(13)	C25	C26	C27	119.31(13)
O6	C27	C26	124.36(13)	O2	C8	C5	119.96(15)
C28	C27	C26	119.68(14)	O2	C8	C9	119.77(14)
C28	C29	C24	120.93(13)	C9	C8	C5	120.27(13)

C18	C19	C20	121.83(13)	C11	C10	C9	121.81(14)
C6	C7	C2	120.39(14)	C10	C11	C12	119.46(14)

Table S7. Hydrogen atom coordinates (Å×10^4) and isotropic displacement parameters (Å^2×10^3) for compound **1**.

Atom	x	y	z	U(eq)
H14	4706.72	1021.92	2681.44	58
H6	4987.31	2185.24	3932.01	57
H21	6157.72	4014.27	6386.54	57
H29	4091.16	3003.51	6983.1	57
H19	8093.52	-194.57	5929.76	60
H7	4527.78	1286.5	5494.77	57
H22	6672.6	4904.29	4829.77	60
H25	6353.38	938.33	9150.28	61
H3	91.71	3108.56	5422.57	60
H4	569.21	4052.44	3860.71	61
H28	1979.35	3907.63	7984.94	59
H13	6713.84	10.89	1645.72	59
H18	8516.53	684.04	4360.55	61
H26	4250.83	1882.37	10157.32	61
H10	4680.25	5146.96	1335.59	66
H11	6766.05	4142.57	335.79	68
H1A	50.93	1379.08	6772.3	111
H1B	202.96	2802.63	7033.74	111
H1C	717.32	1233.41	7678.96	111
H16A	8509.35	3150.18	2238.93	115
H16B	7985.15	1858.78	2925.7	115
H16C	9549.41	2030.62	2954.48	115
H30A	2321.21	3585.86	10860.23	124

H30B	1707.81	2250.68	10898.38	124
H30C	586.21	3856.58	10969.59	124
H15A	8162.83	2700.36	-839.91	136
H15B	9725.89	1479.51	-733.05	136
H15C	9185.25	2800.73	-173.47	136

Table S8. Excitation properties, oscillator strengths (f) & dominant electronic transitions of compound **1** calculated at the TD-B3LYP/6-31++G(d,p) level.

Transition	ΔE (eV)	λ (nm)	f	Configuration (orbital symmetry)	Coefficient
S_0 _ S_1	3.6462	340.04	0.0025	HOMO (124) _ LUMO (129)	0.37071
S_0 _ S_2	3.6492	339.76	0.0039	HOMO (123) _ LUMO (129)	0.39563
S_0 _ S_3	4.1373	299.68	0.0430	HOMO (126) _ LUMO (129)	0.42428
S_0 _ S_4	4.1715	297.22	0.8469	HOMO (126) _ LUMO (129)	0.39568
S_0 _ S_5	4.1737	297.06	0.0308	HOMO (128) _ LUMO (129)	0.61393
S_0 _ S_6	4.2727	290.17	0.0000	HOMO (126) _ LUMO (130)	0.51700
S_0 _ T_1	0.4835	2564.37	0.0229	HOMO (127B) _ LUMO (128B)	0.97741
S_0 _ T_2	0.5773	2147.49	0.0048	HOMO (124B) _ LUMO (128B)	0.94839
S_0 _ T_3	0.9641	1286.08	0.0000	HOMO (126B) _ LUMO (128B)	0.99270
S_0 _ T_4	1.2235	1013.37	0.0001	HOMO (125B) _ LUMO (128B)	0.99307
S_0 _ T_5	1.2784	969.87	0.0000	HOMO (129A) _ LUMO (130A)	0.99910
S_0 _ T_6	1.2895	961.51	0.0006	HOMO (122B) _ LUMO (128B)	0.51700

Table S9. Excitation properties, oscillator strengths (f) & dominant electronic transitions of compound **5** calculated at the TD-B3LYP/6-31++G(d,p) level.

	ΔE (eV)	λ (nm)	f	Configuration (orbital symmetry)	Coefficient
S_0 _ S_1	3.1854	389.23	0.1261	HOMO (80) _ LUMO (81)	0.69422
S_0 _ S_2	3.7576	329.95	0.0054	HOMO (79) _ LUMO (81)	0.67437
S_0 _ S_3	3.9784	311.64	0.0038	HOMO (78) _ LUMO (81)	0.65713
S_0 _ S_4	4.0655	304.97	0.0302	HOMO (77) _ LUMO (81)	0.50732

S_0 _ S_5	4.5322	273.56	0.2071	HOMO (76) _ LUMO (81)	0.63920
S_0 _ S_6	4.6381	267.32	0.8008	HOMO (80) _ LUMO (82)	0.46378

Table S10. Photophysical properties of **5@1**.

λ_{abs}	365 nm
$\lambda_{\text{fluorescence}}$	496 nm
$\lambda_{\text{phosphorescence}}$	557 nm
Φ_{f}	0.189
$\tau_{\text{fluorescence}}$	22.77 ns
$\Phi_{\text{phosphorescence}}$	0.08
$\tau_{\text{phosphorescence}}$	1.49 ms
$k_{\text{fluorescence}}$	8.31×10^{6} s^{-1}
k_{nr}	4.38×10^{9} s^{-1}
$k_{\text{phosphorescence}}$	67.22 s^{-1}
k_{nr}	603.92 s^{-1}

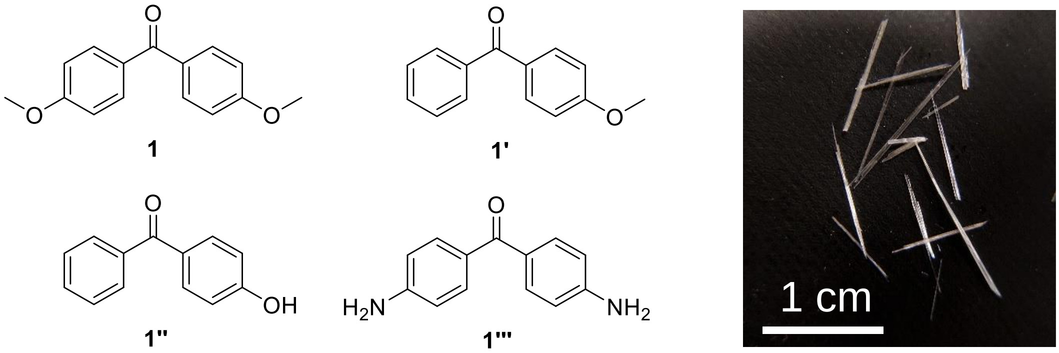

Fig. S1. Chemical structures of 4,4’-dimethoxybenzophenone (**1**), 4-methoxybenzophenone (**1’**), 4,4'-diaminobenzophenone (**1’’**) and 4-hydroybenzophenone (**1’’’**) and a digital photograph of the crystals of 4-hydroybenzophenone.

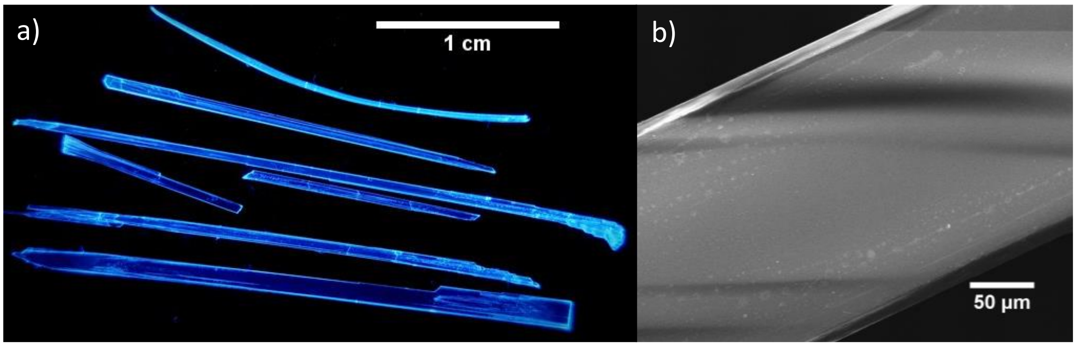

Fig. S2. a) Photographs under UV light and b) SEM images of the crystals of **1**.

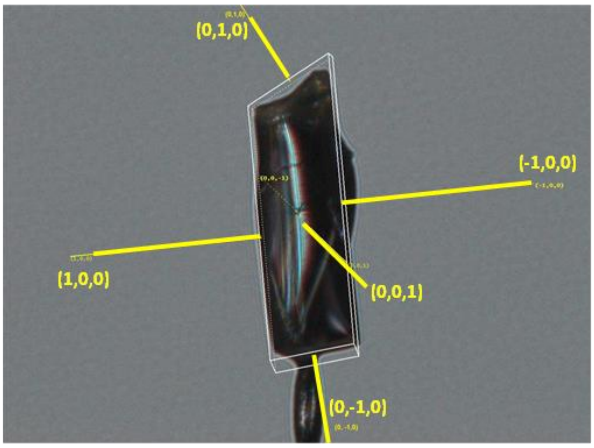

Fig. S3. Face indexing of the crystals of **1**.

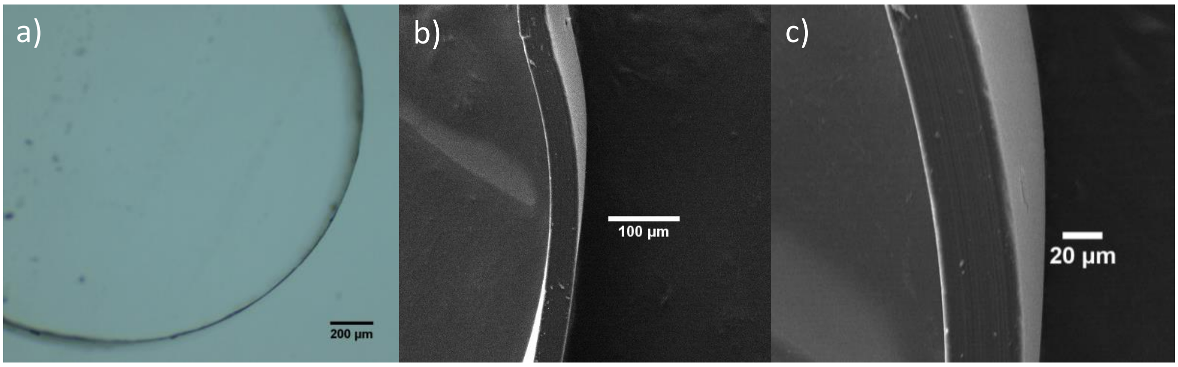

Fig. S4. SEM images of the crystals of **1** in the bent state.

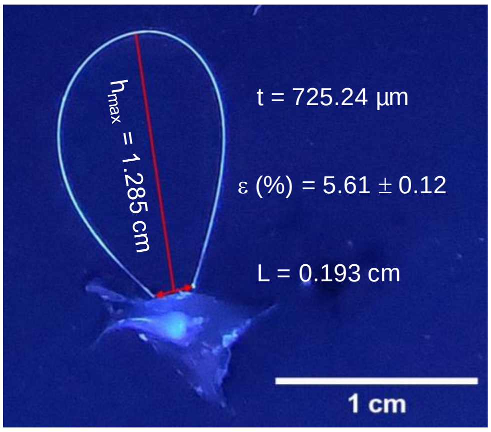

Fig. S5. Bending strain calculation of the crystals of **1**.

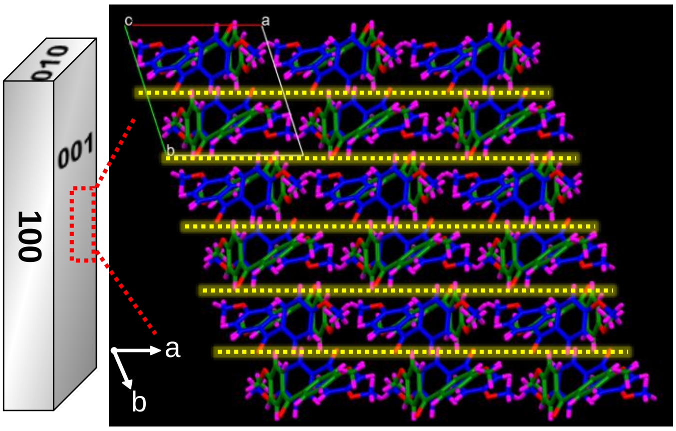

Fig. S6. Crystal packing in **1** viewed along crystallographic *c*-axis showing the direction of the slip panes as yellow dotted lines.

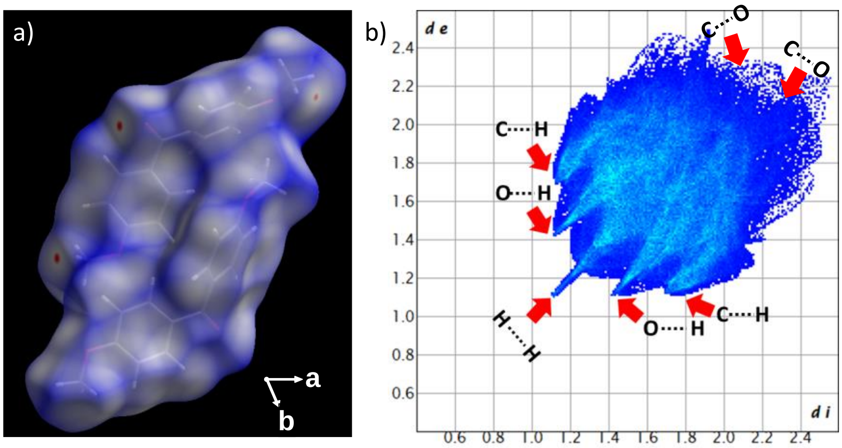

Fig. S7. a) Hirshfeld surface analysis of **1** and b) Hirshfeld 2D fingerprint plot of **1**.

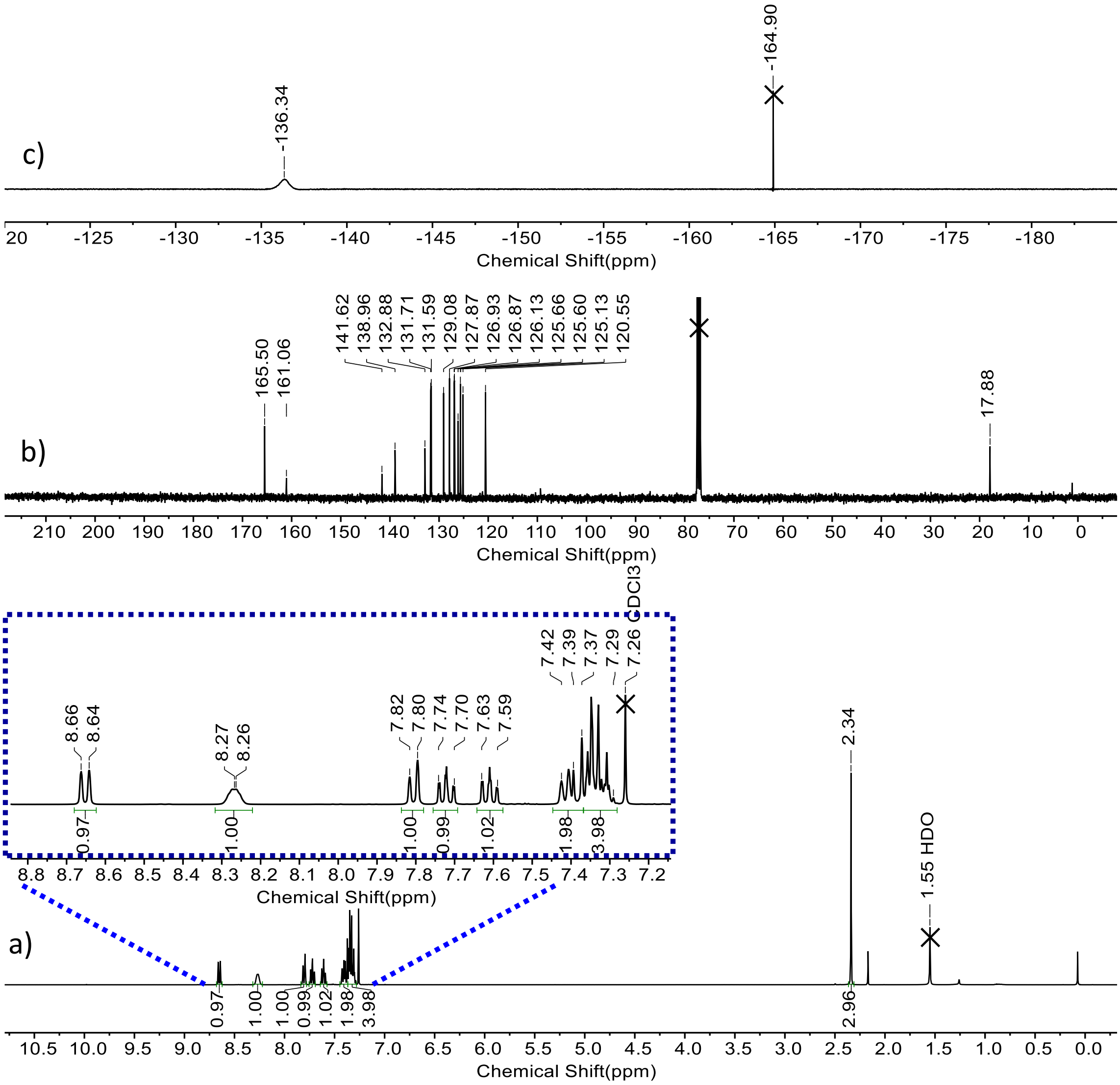

Fig. S8. a) ^{1}H, b) ^{13}C and c) ^{19}F NMR spectra of **5** in $CDCl_3$ at 298 K. Selected regions of the spectra are enlarged as insets in (a).

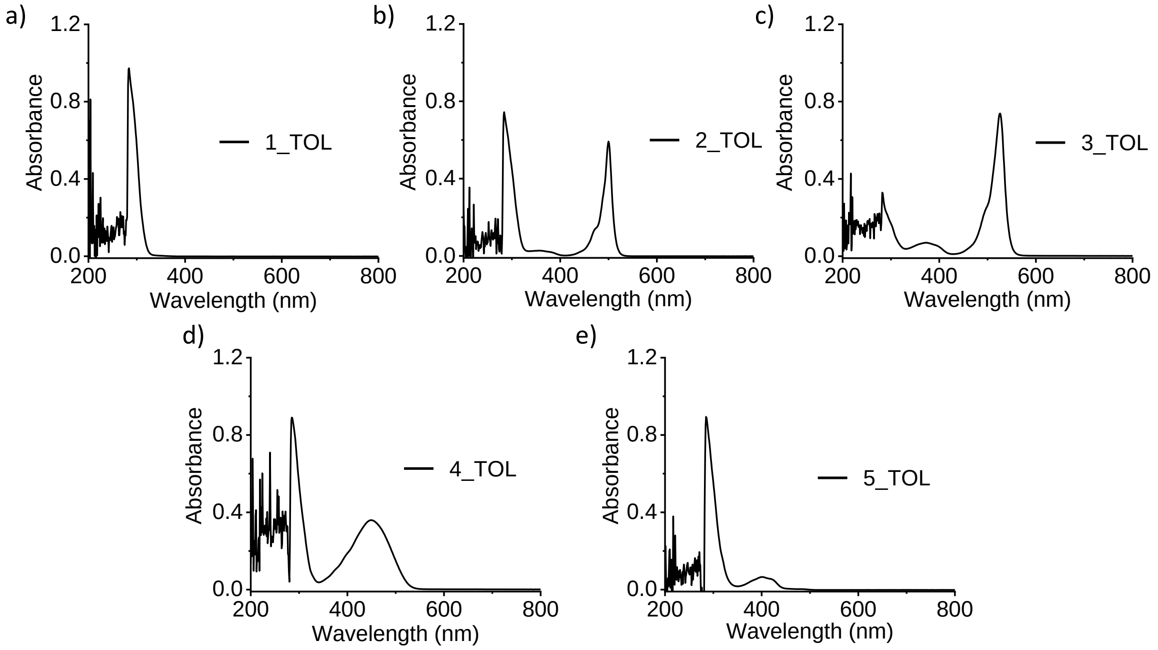

Fig. S9. a-e) UV-Visible absorption spectra of **1-5** (10 μM) in toluene.

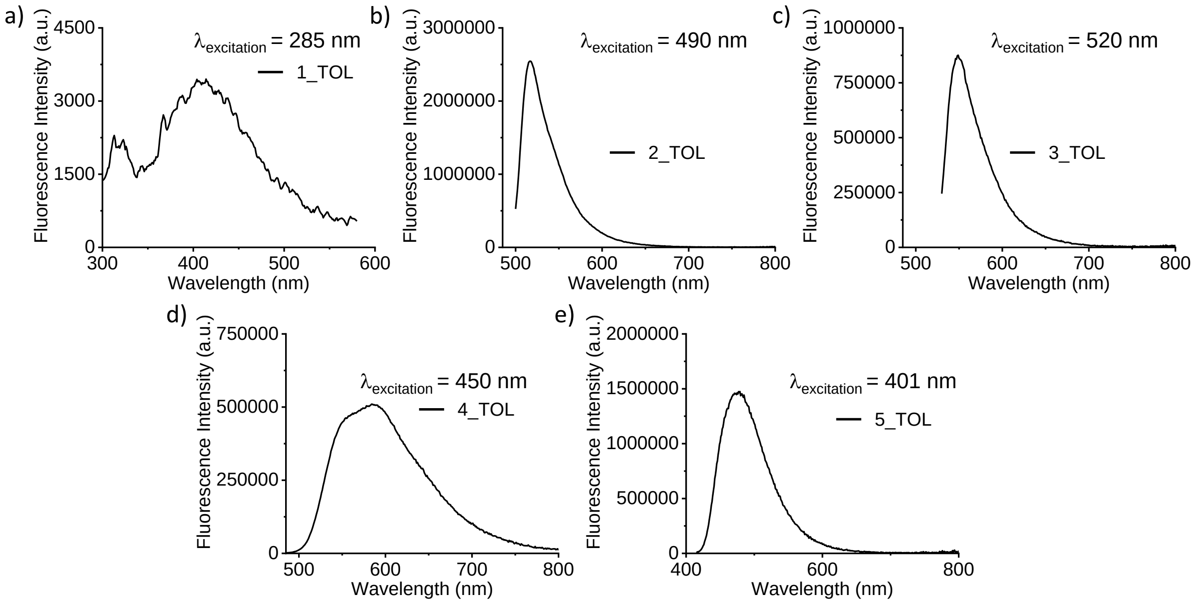

Fig. S10. a-e) Fluorescence spectra of **1-5** (10 μM) in toluene.

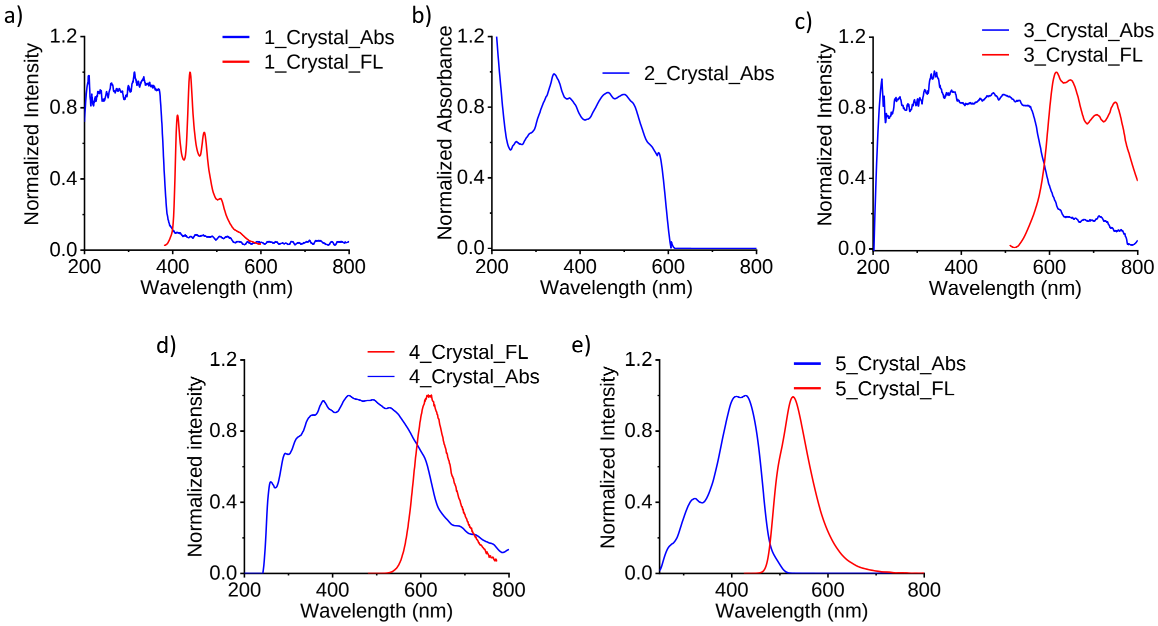

Fig. S11. a-e) Normalized UV-Visible absorption and fluorescence spectra of **1-5** in the single crystalline state. Excitation wavelength, (a) 365, (c) 500, (d) 450 and (e) 415 nm.

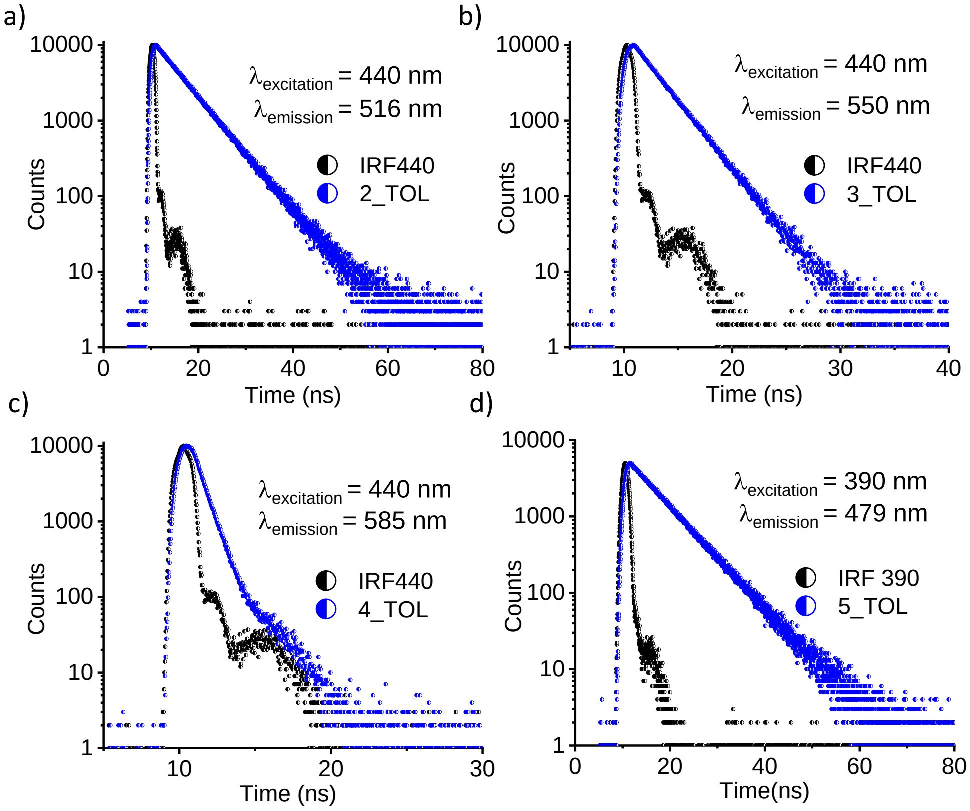

Fig. S12. a-d) Fluorescence lifetime decay profiles of **2-5** (10 μM) in toluene.

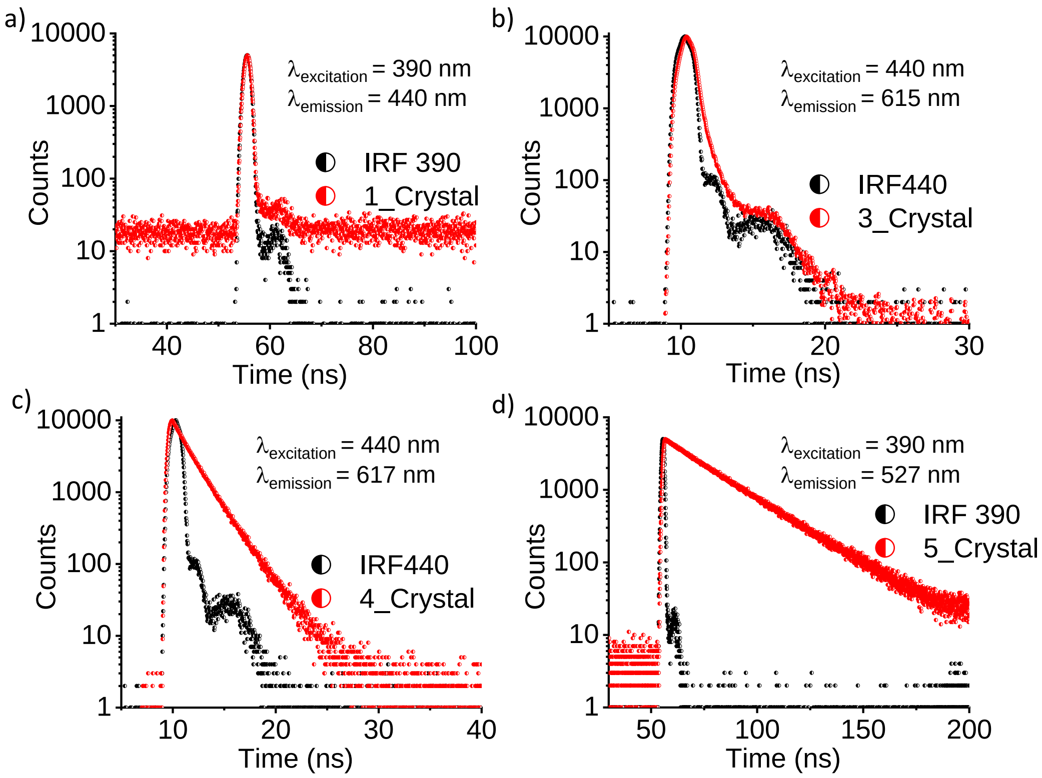

Fig. S13. Fluorescence lifetime decay profiles of **1** and **3-5** in the single crystalline state.

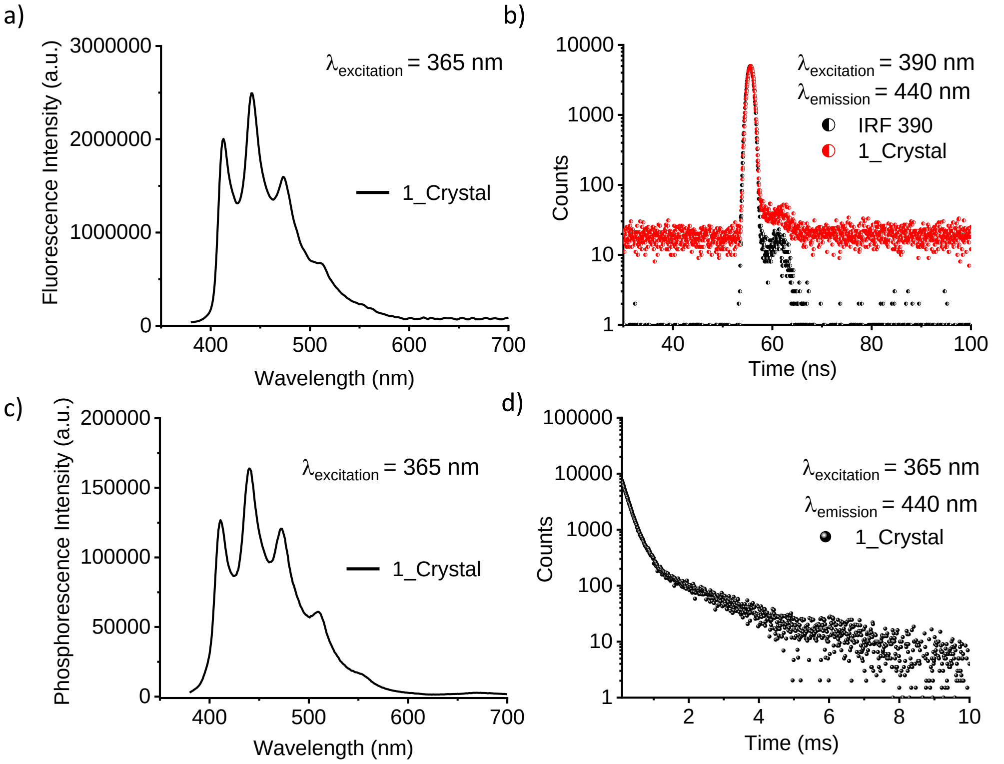

Fig. S14. Fluorescence (a) spectrum and (b) decay profile and phosphorescence (c) spectrum and (d) decay profile of **1** in the single crystalline state. Phosphorescence was measured with a delay of 0.1 ms.

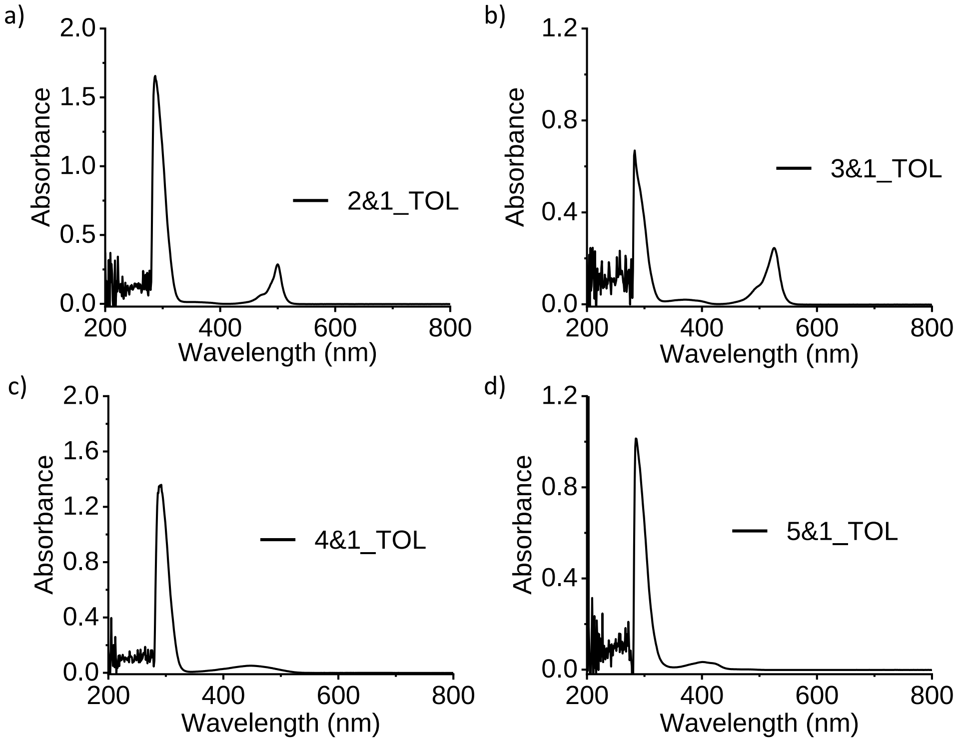

Fig. S15. a-d) UV-Visible absorption spectra of a mixture of **1** (10 µM) and **2**-**5** (10 µM) in toluene.

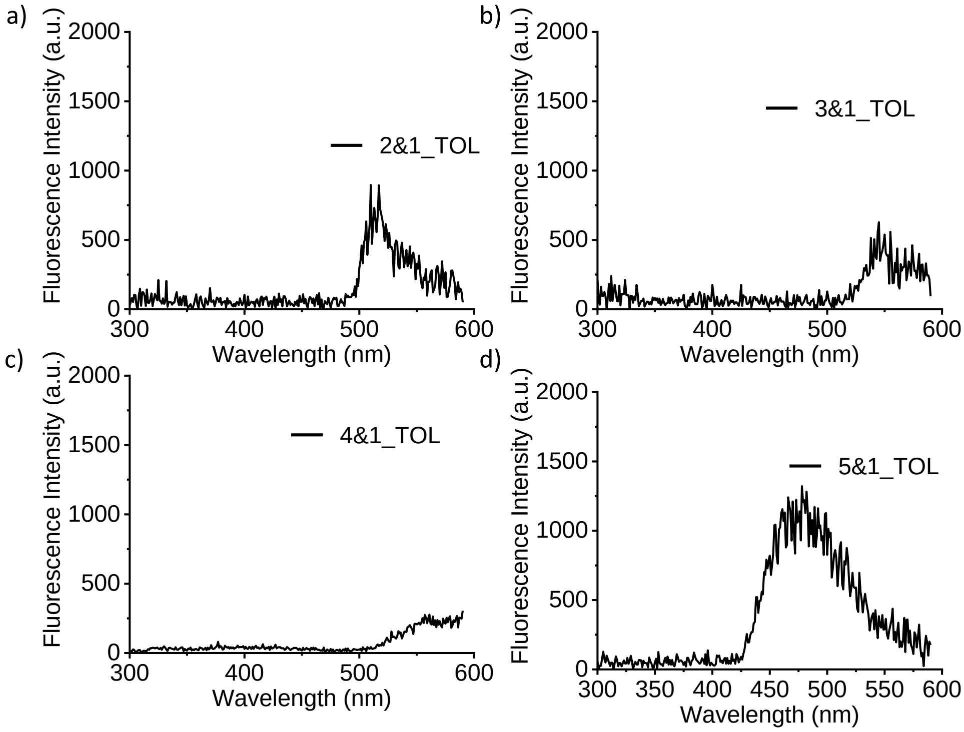

Fig. S16. a-d) Fluorescence spectra of a mixture of **1** (10 µM) and **2**-**5** (10 µM) in toluene. Excitation wavelength, 285 nm.

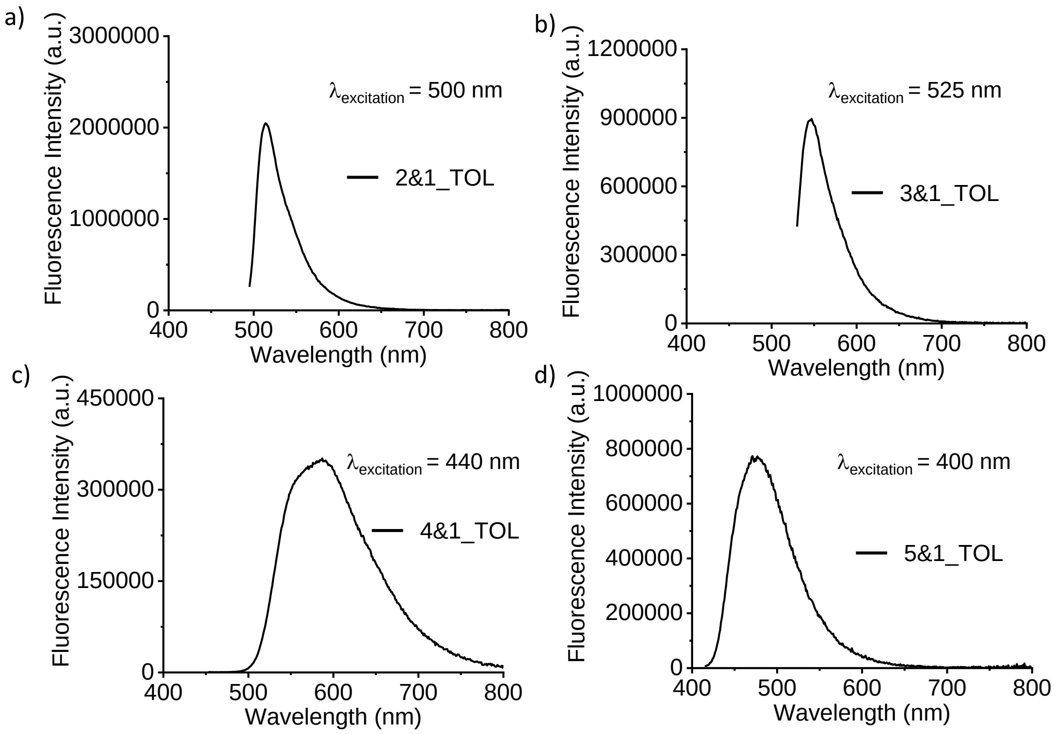

Fig. S17. a-d) Fluorescence spectra of a mixture of **1** (10 μM) and **2**-**5** (10 μM) in toluene. Excitation wavelength: (a) 500, (b) 525, (c) 440 and (d) 400 nm.

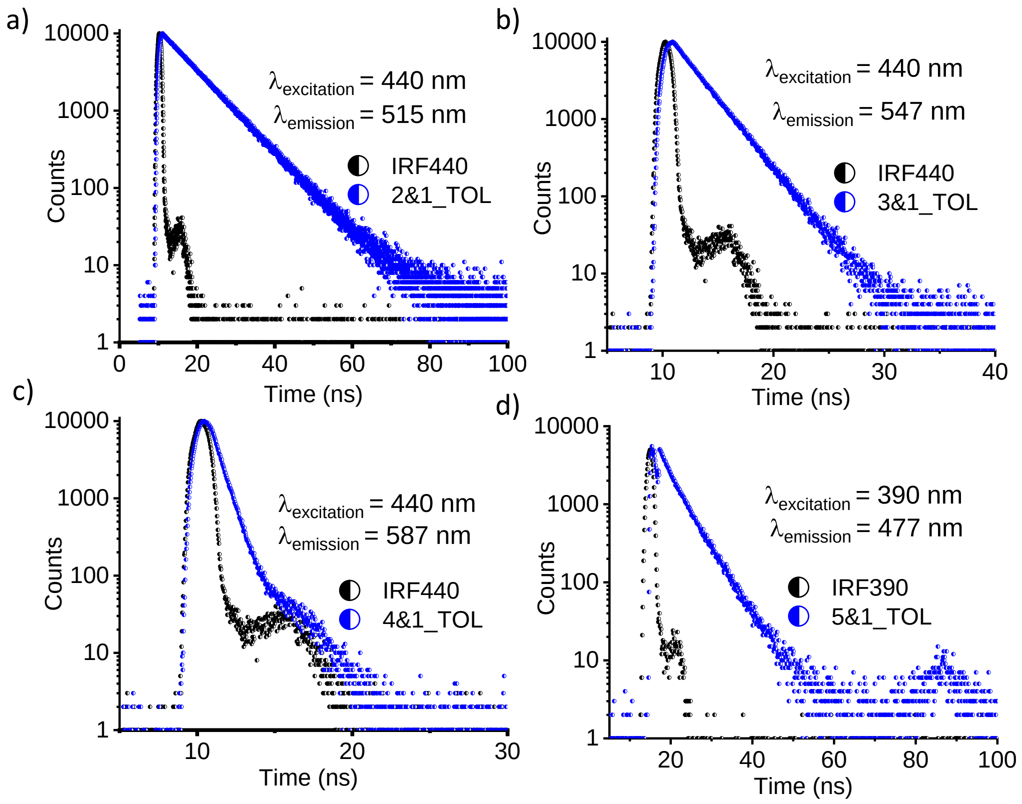

Fig. S18. a-d) Fluorescence lifetime decay profiles of a mixture of **1** (10 μM) and **2**-**5** (10 μM) in toluene.

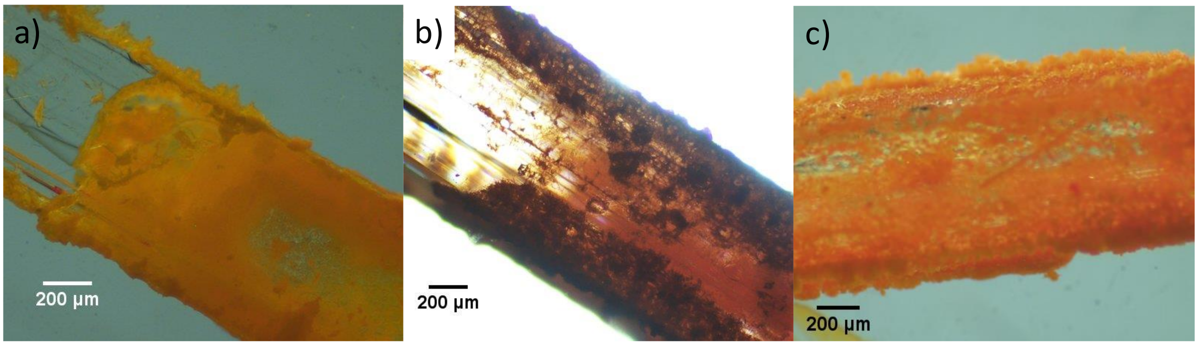

Fig. S19. Optical microscope images of the crystal of **1** coated with (a-c) **2-4,** respectively.

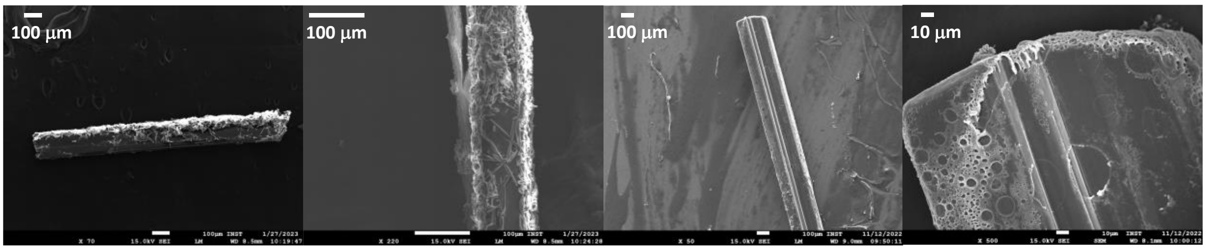

Fig. S20. SEM images of the coated crystal **5@1**.

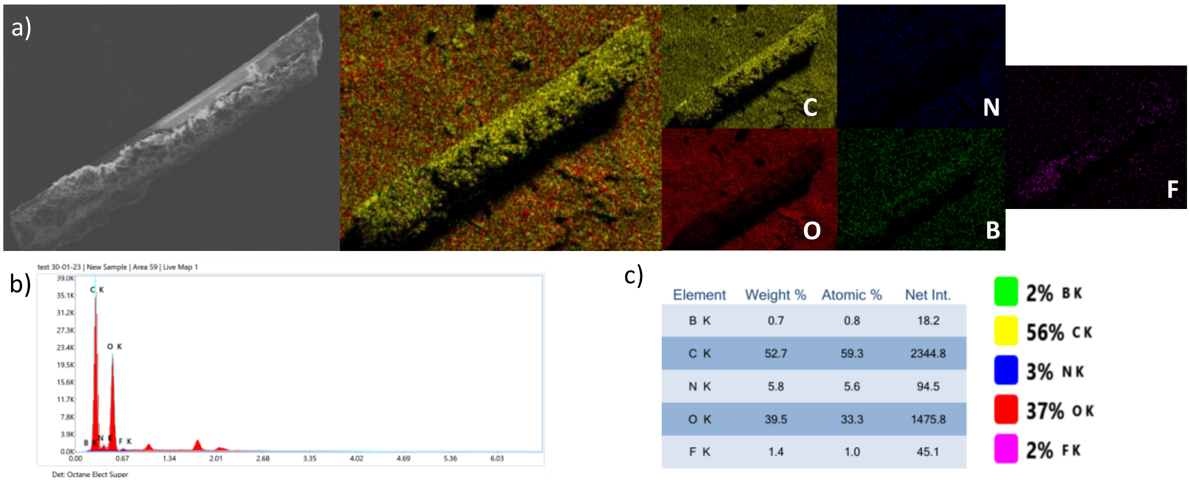

Element	Weight %	Atomic %	Net Int.
B K	0.7	0.8	18.2
C K	52.7	59.3	2344.8
N K	5.8	5.6	94.5
O K	39.5	33.3	1475.8
F K	1.4	1.0	45.1

Fig. S21. a) EDX mapping, b) spectra and c) the respective quantitative results of the coated crystal **5@1**.

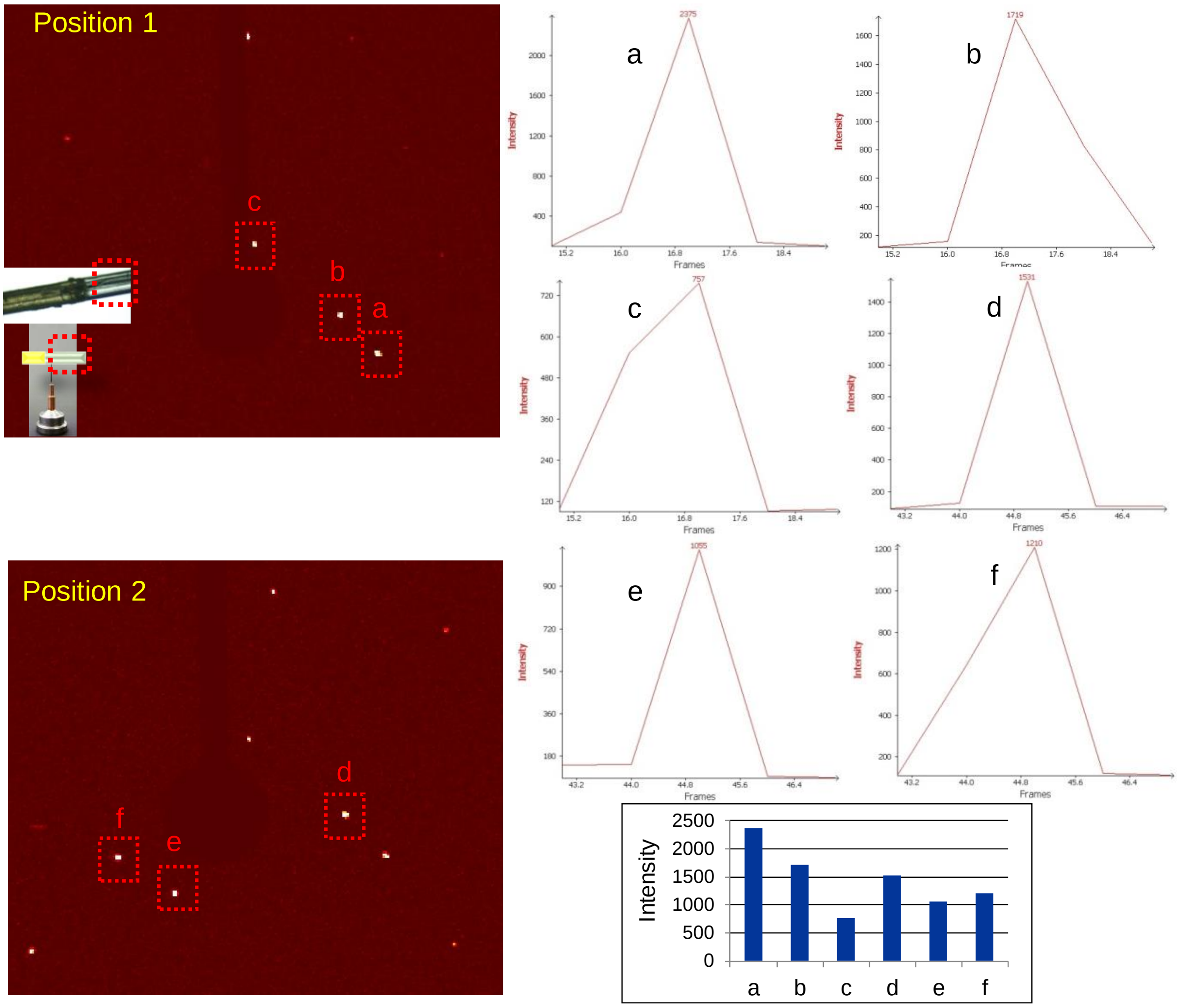

Fig. S22. Single crystal X-ray diffraction pattern of crystal **5@1** at the uncoated position.

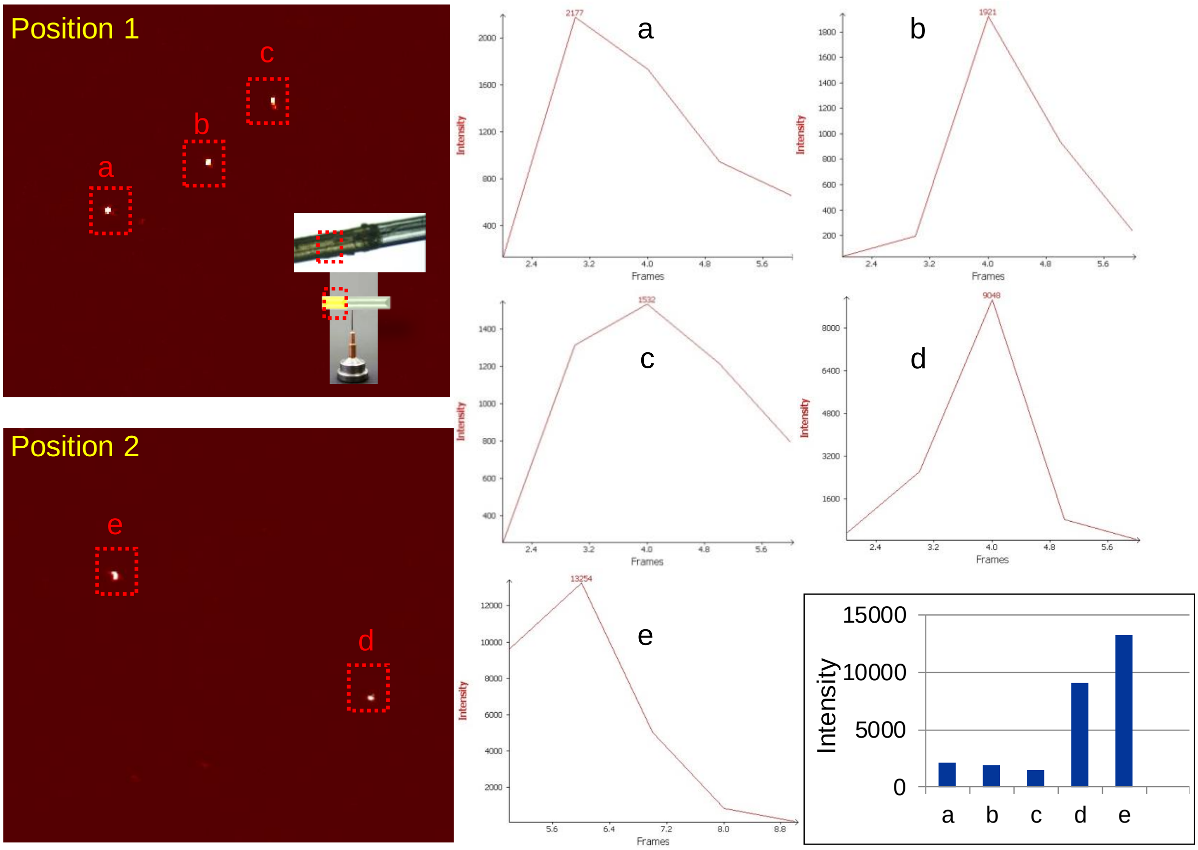

Fig. S23. Single crystal X-ray diffraction pattern of crystal **5@1** at the coated position.

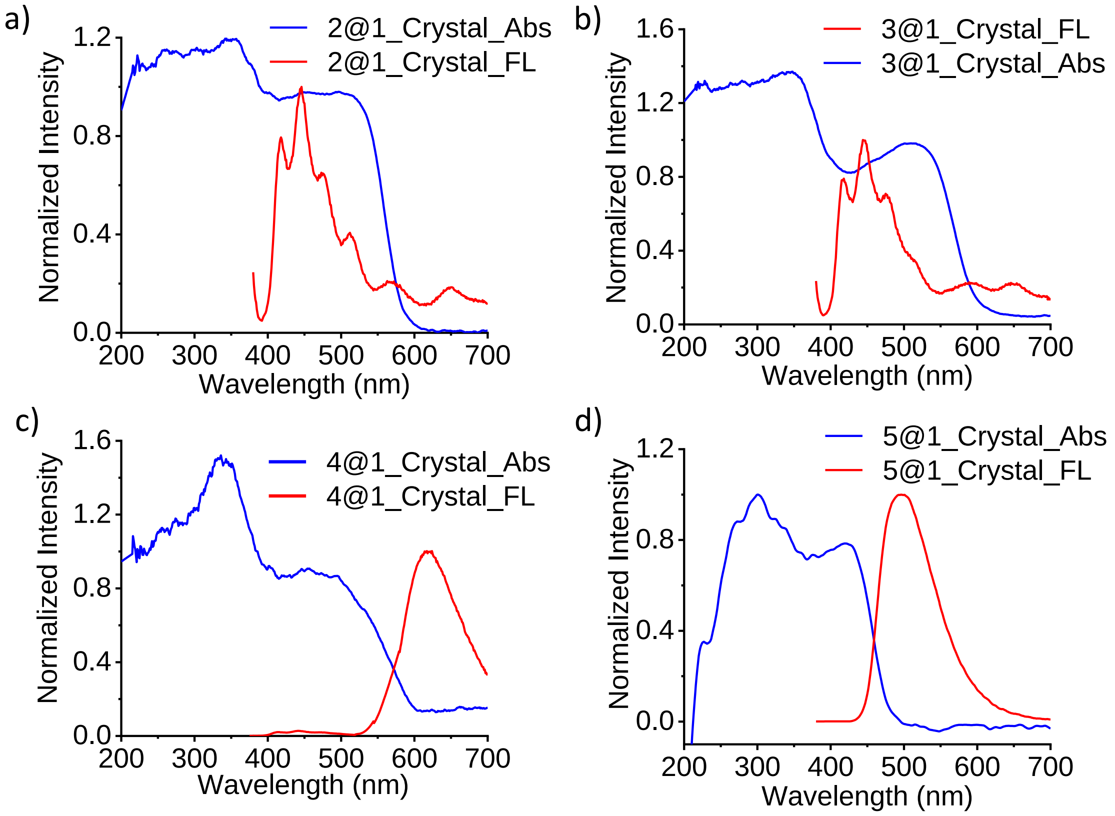

Fig. S24. a-d) Normalized UV-Visible absorption and fluorescence spectra of **2@1, 3@1, 4@1** and **5@1**. Excitation wavelength, 365 nm.

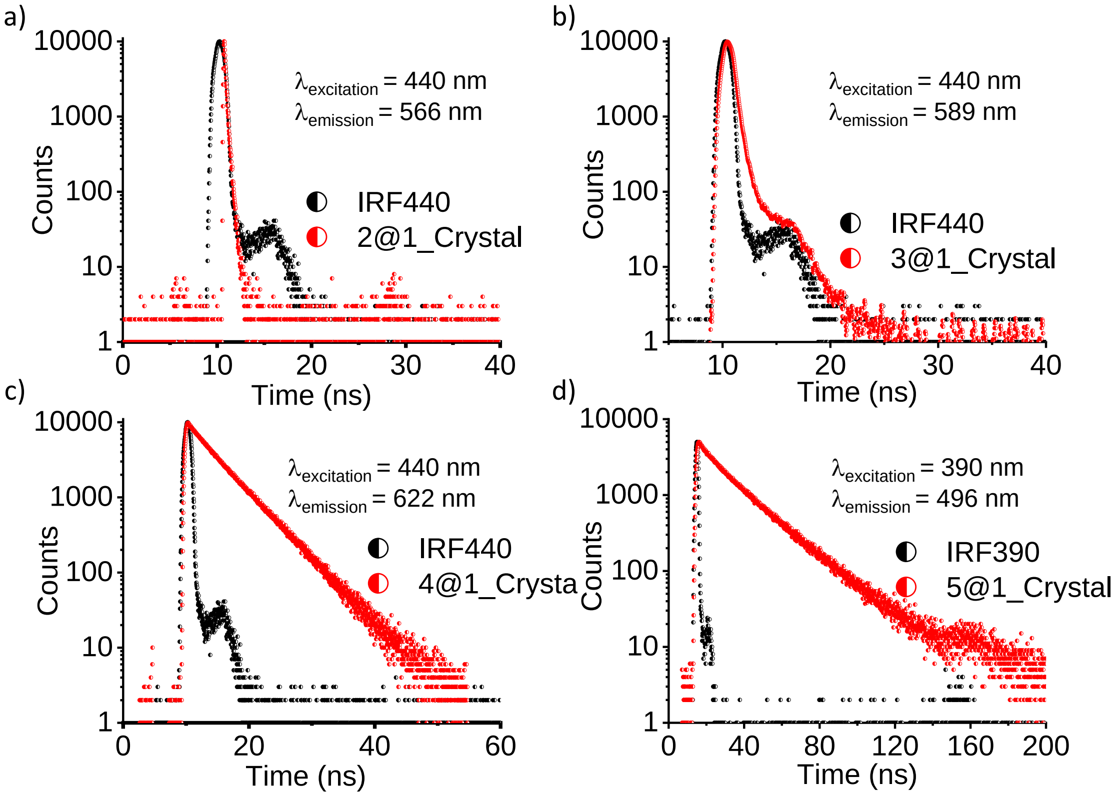

Fig. S25. Fluorescence lifetime decay profiles of **2@1**, **3@1**, **4@1** and **5@1**.

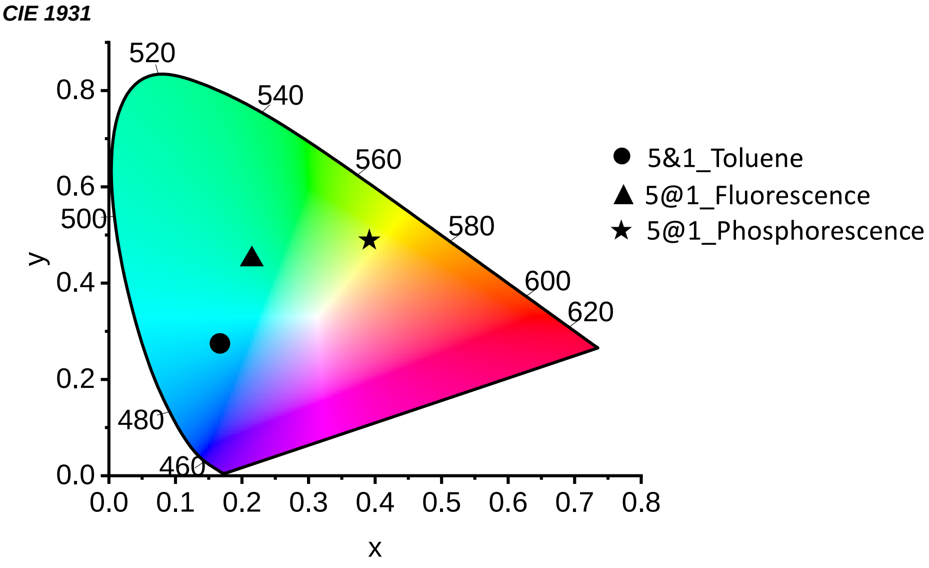

Fig. S26. *CIE* plot of a mixture of **1** and **5** in toluene and the coated crystals **5@1**.

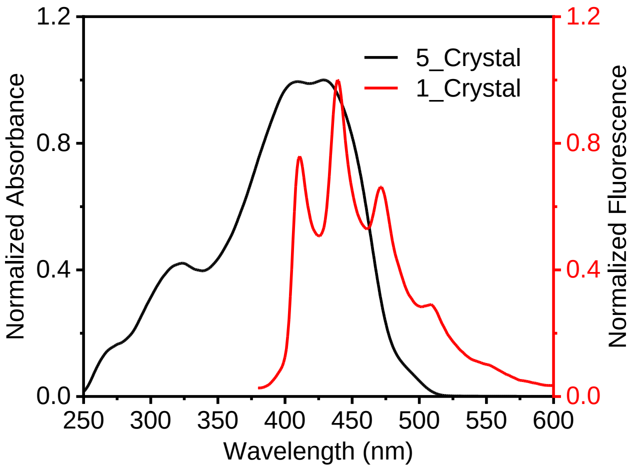

Fig. S27. Normalized absorption and fluorescence spectra of the crystals of **5** and **1**, respectively.

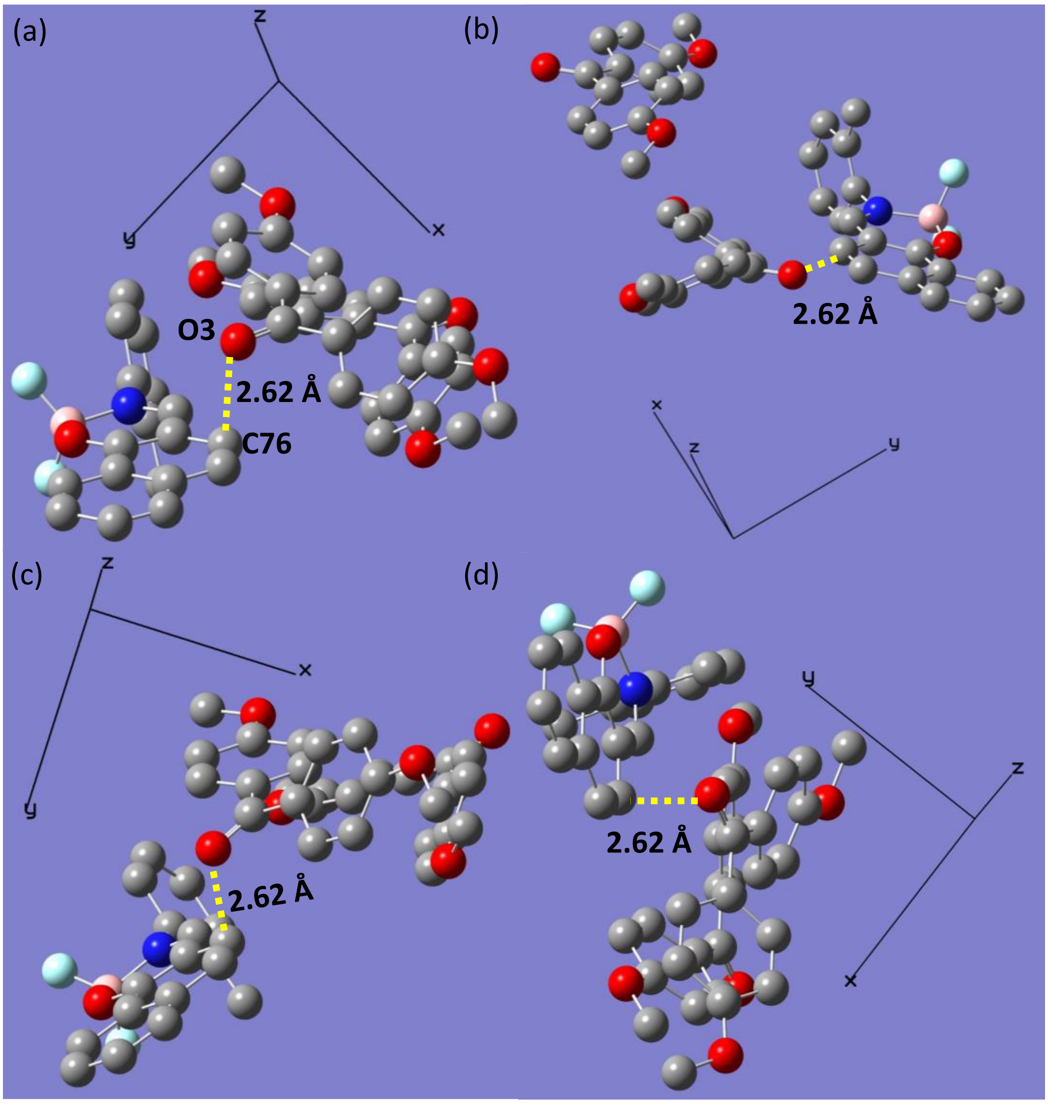

Fig. S28. Interactions between **5** and **1** obtained computationally.

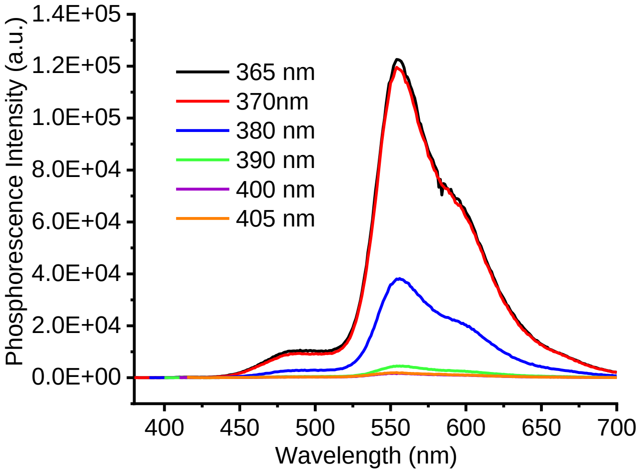

Fig. S29. Phosphorescence spectra of the crystal **5@1** obtained using different excitation wavelengths. Delay time, 0.1 ms.

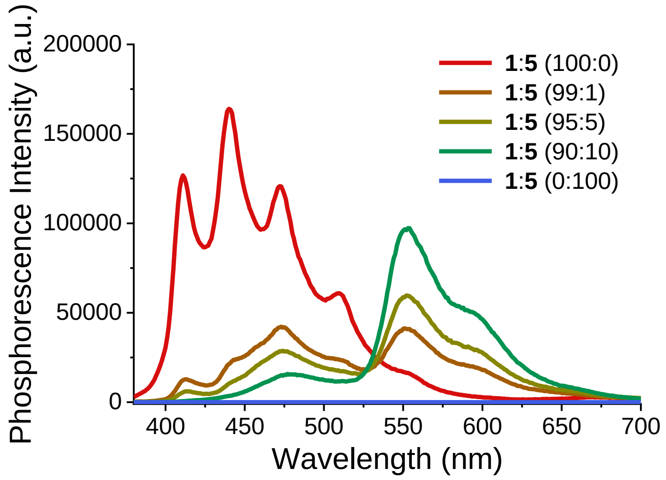

Fig. S30. Phosphorescence spectra of thin films of mixtures of **1** and **5**. Excitation wavelength, 365 nm; delay time, 0.1 ms.

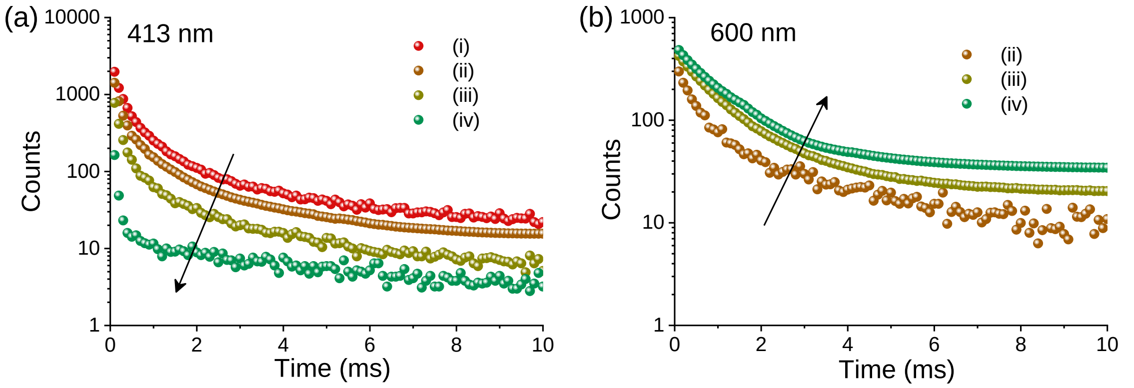

	Mol% **1** : Mol% **5**	Average lifetime at 413 nm
i	100 : 0	0.327 ms
ii	99 : 1	0.206 ms
iii	95 : 5	0.08 ms
iv	90 : 10	Not detected
v	0 : 100	No phosphorescence

	Mol% **1** : Mol% **5**	Average lifetime at 600 nm
i	100 : 0	No phosphorescence
ii	99 : 1	0.642 ms
iii	95 : 5	0.938 ms
iv	90 : 10	1.01 ms
v	0 : 100	No phosphorescence

Fig. S31. Phosphorescence decays at (a) 413 and (b) 600 nm of thin films of mixtures of **1** and **5**. Tables below each plot shows the composition and the average lifetime of the mixture. Excitation wavelength, 365 nm; delay time, 0.1 ms.

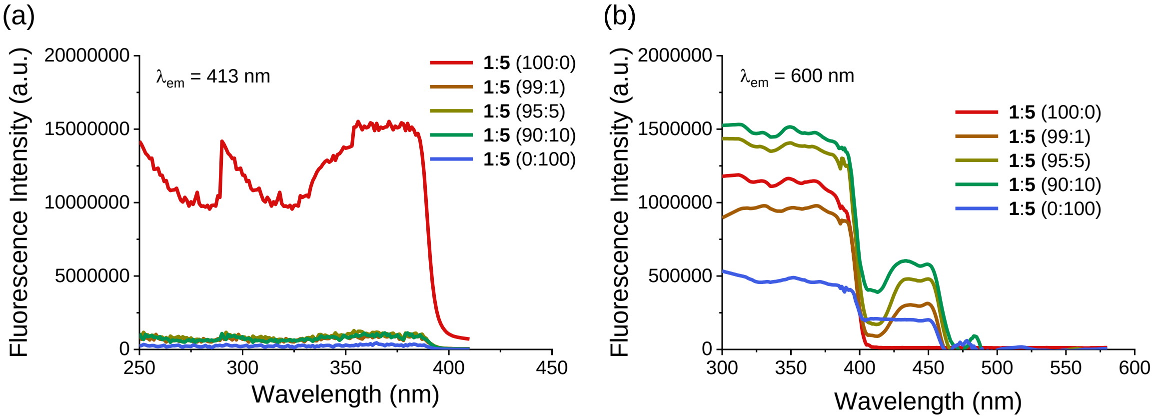

Fig. S32. Fluorescence excitation spectra collected at (a) 413 and (b) 600 nm of thin films of mixtures of **1** and **5**.

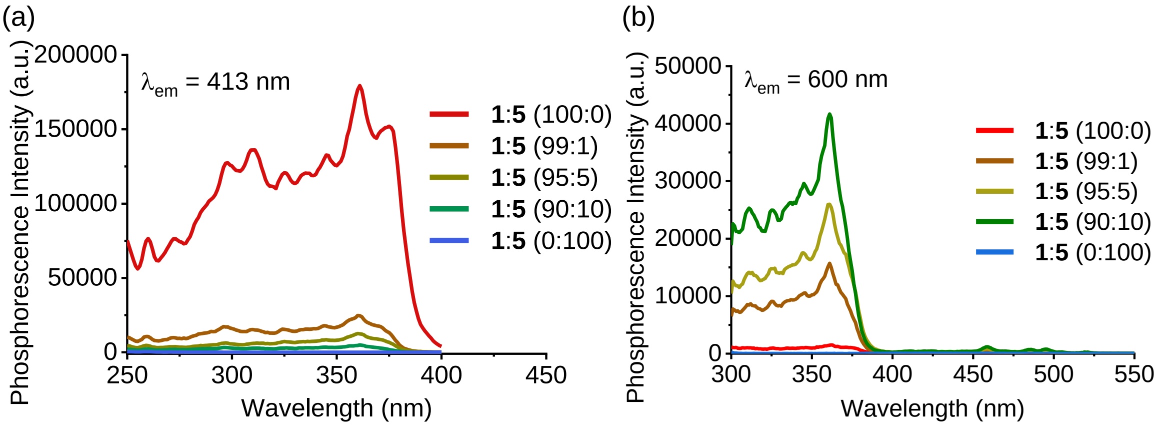

Fig. S33. Phosphorescence excitation spectra collected at (a) 413 and (b) 600 nm of thin films of mixtures of **1** and **5**. Delay time, 0.1 ms.

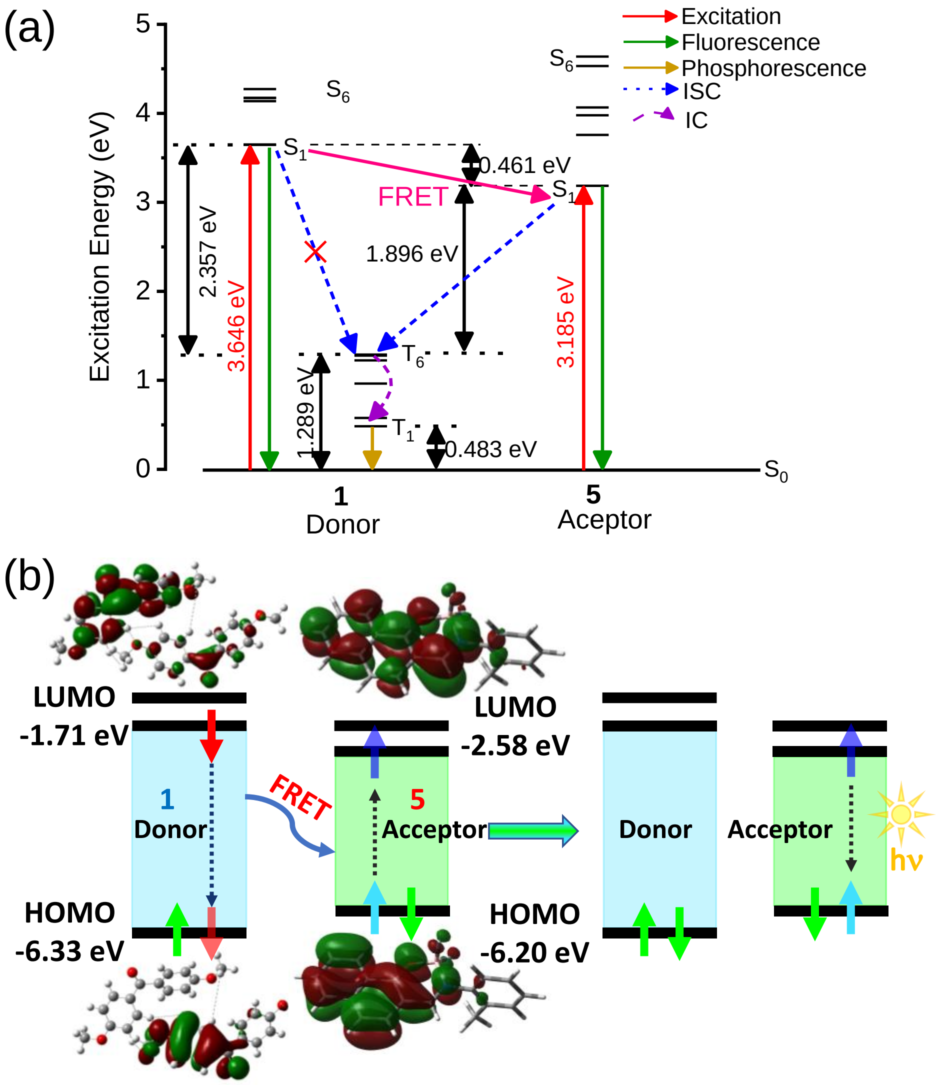

Fig. S34. Schematic diagram of the photophysical processes occurring in a mixture of **1** and **5**.

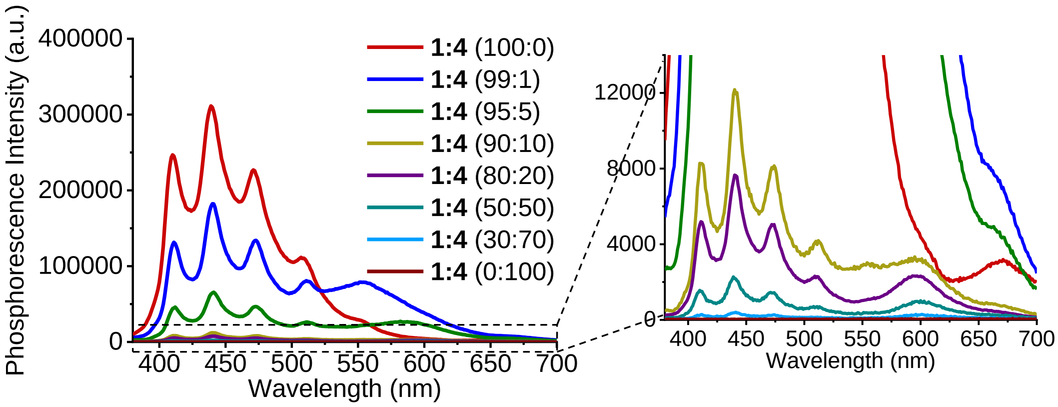

Amount of **4** or **5** in the mixture of **1** and **4/5**	Decrease in emission intensity at 413 nm	
	4	5
1 mol%	49%	90%
5 mol%	83%	95%
10 mol%	96%	99%

Fig. S35. Phosphorescence spectra of thin films of mixtures of **1** and **4**. Table shows the decrease in the emission intensity at 413 nm at different mol% of **4** or **5** in a mixture of **1** and **4** or **5**. Excitation wavelength, 365 nm; delay time, 0.1 ms.

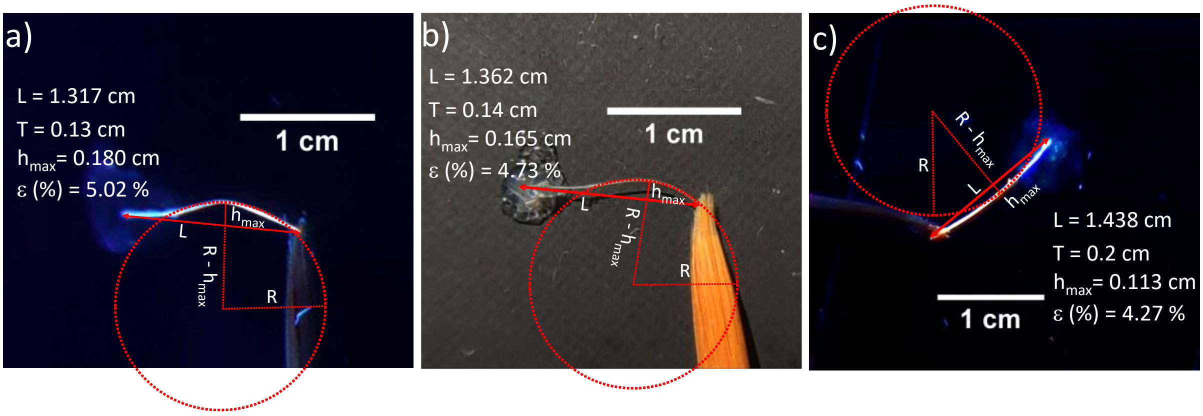

Fig. S36. a-c) Bending strain calculation of the coated crystals **2@1**, **3@1** and **4@1** respectively.

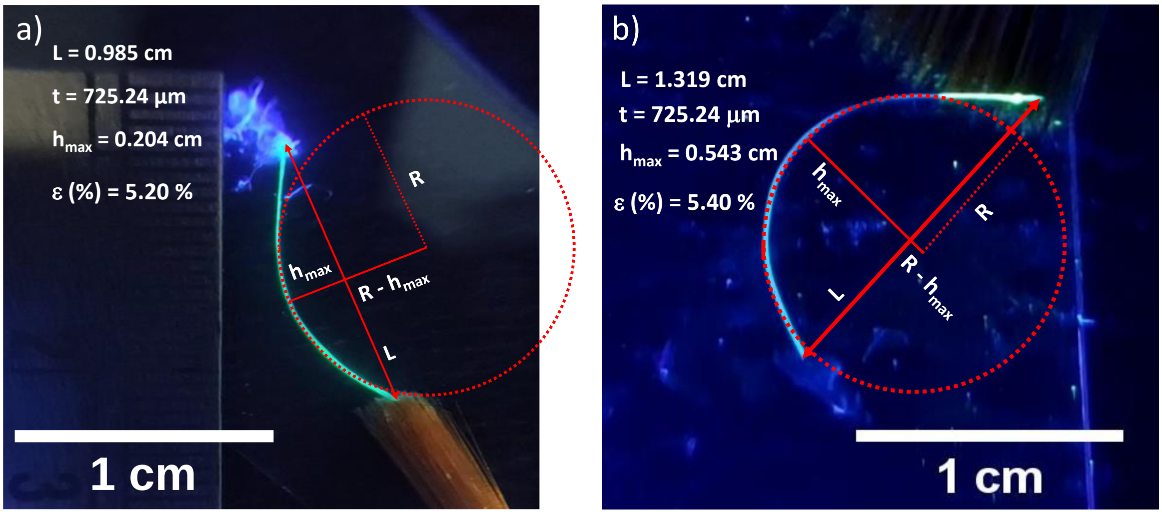

Fig. S37. Bending strain calculation of the crystal **5@1** using a) completely and b) partially coated crystals.

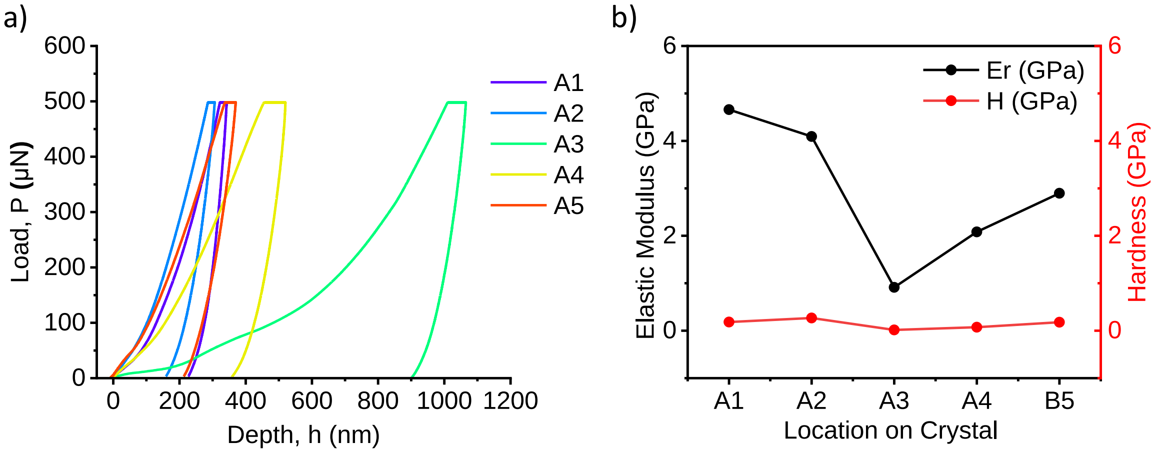

Fig. S38. Nanoindentation measurement impacted on the (100) plane of the crystals of **1**. Plot of a) *P*–*h* curves and plots of b) elastic modulus, *E* and hardness, *H*, calculated for the pristine crystal **1**.

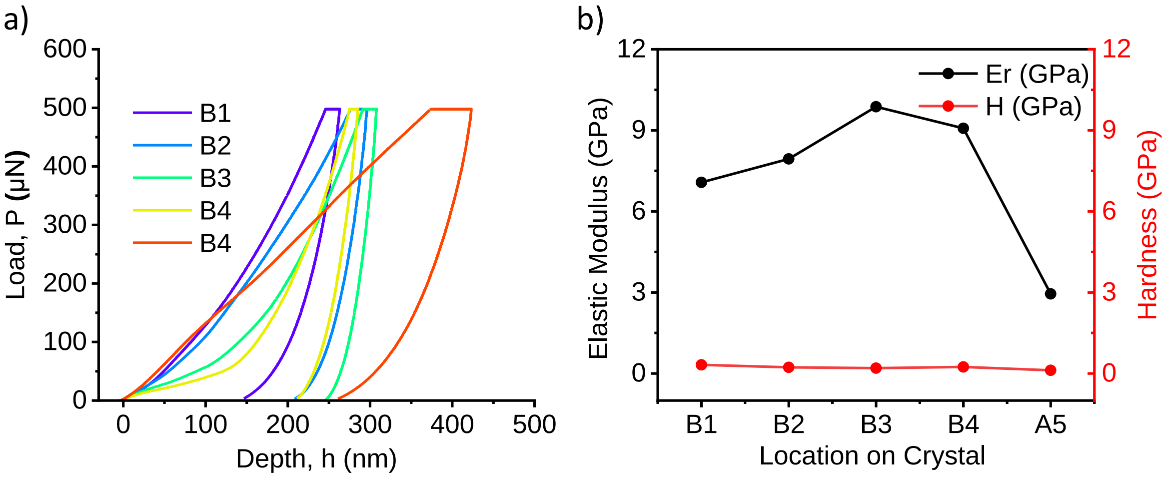

Fig. S39. Nanoindentation measurement impacted on the (100) plane of coated crystal **5@1**. Plot of a) *P*–*h* curves and plot of b) elastic modulus, *E* and hardness, *H*, calculated for the coated crystal **5@1**.

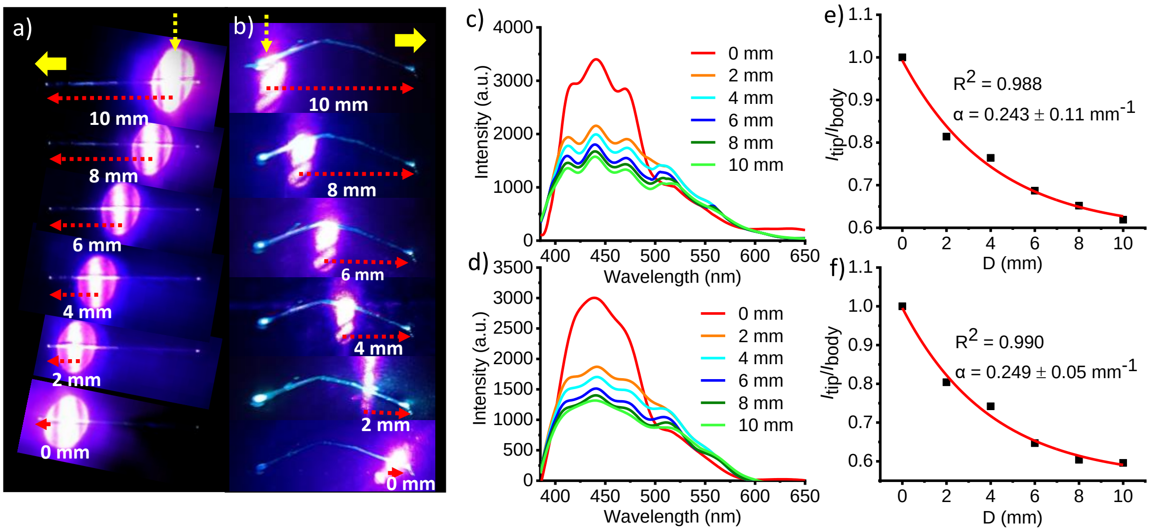

Fig. S40. Photographs showing the optical waveguiding properties of a) straight and b) bent crystals excited with 365 nm laser focused at different positions. Emission spectra collected at the tip of a crystal of **1** in the c) straight or d) bent state with the distance between the tip and the excitation site changed gradually. The point of light incidence is shown with dotted yellow arrows and the end at which the propagated light was captured is indicated with block yellow arrows. e, f) Single-exponential fits of I_{tip} / I_{body} with increasing tip to excitation distance plotted for straight and bent crystals, respectively.

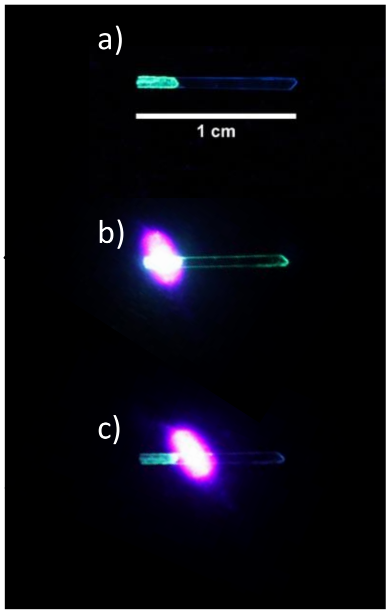

Fig. S41. Digital photographs of the coated crystals **5@1** a) under UV light and upon excitation at b) coated part and c) uncoated part by using a 365 nm laser.

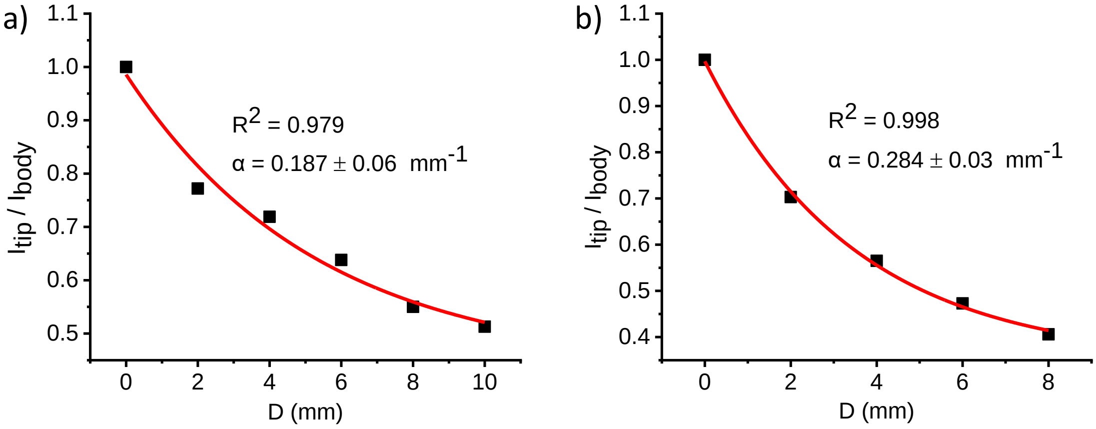

Fig. S42. The I_{tip} / I_{body} decays of the coated crystals **5@1** in the a) straight and b) elastically bent state.

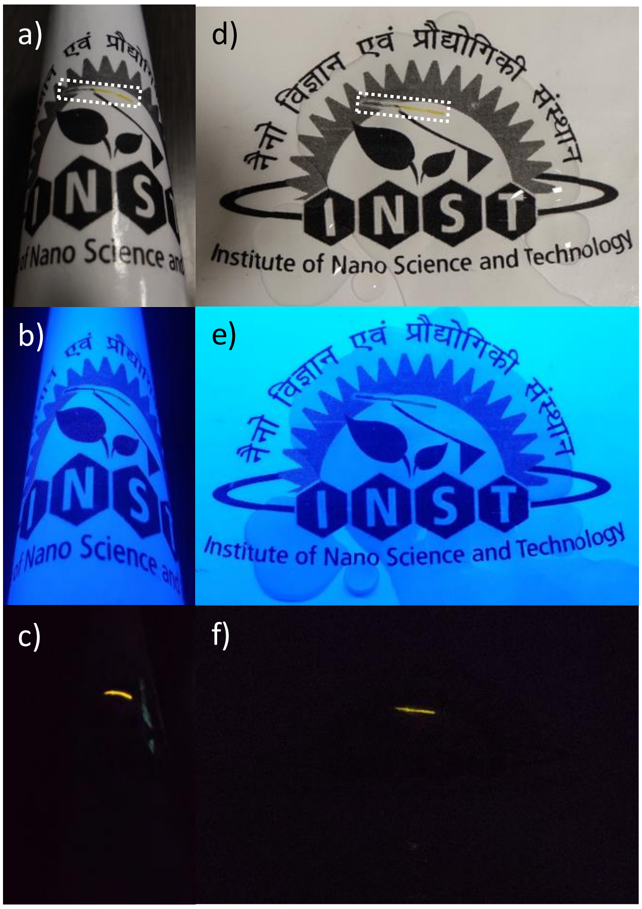

Fig. S43. Digital images of documents embedding the coated crystals **5@1** showing bending and after washing under a, d) ambient light, b, e) UV on and c, f) UV off state.

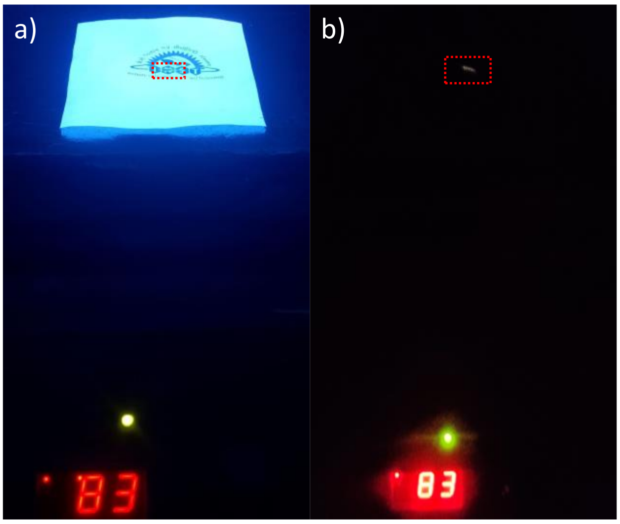

Fig. S44. Digital images of documents embedding the coated crystals **5@1** at higher temperature under a) UV light and b) after turning off the UV light.

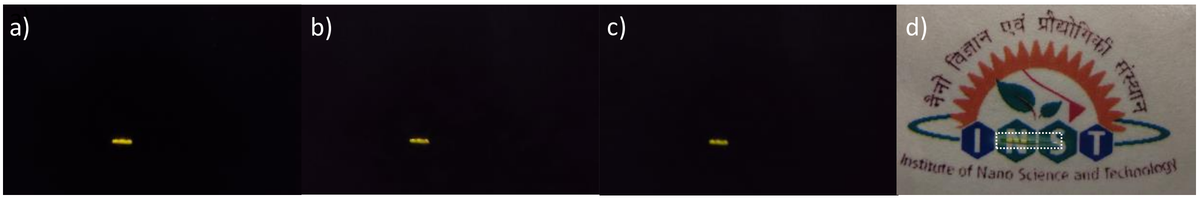

Fig. S45. Digital images of the document embedding the crystal **5@1** captured after 50 ms after turning off the UV light. The document was aged for a) 15, b) 30 and c) 60 days. A digital image of the document under daylight is shown in (d) as a reference for the position of the crystal. The length of the crystal embedded in the document is 1 cm.